TUSKEGEE INSTITUTE

SCHOOL OF MECHANICAL ENGINEERING

TUSKEGGE INSTITUTE, ALABAMA

STEADY-STATE AND TRANSIENT OPERATION OF A HEAT-PIPE RADIATOR SYSTEM

CONTRACT NO. NAS9-13844

BY

JOHN P. SELLERS

SPONSORED BY

ENVIRONMENTAL AND THERMAL SYSTEMS SECTION

MANNED SPACECRAFT CENTER

NATIONAL AERON AUTICS AND SPACE ADMINISTRATION

HOUSTON, TEXAS

DECEMBER, 1974

FOREWARD

This report was prepared for Johnson Space Center of the National Aeronautics and Space Administration. The work was performed under Contract NAS9-13844 with Mr. W. Ellis and Mr. B. French providing NASA guidance.

The work was performed from January 1974 to August 1974. The author would like to acknowledge the assistance of Mr. B. Carroll, Lockheed Electronics Company, Inc. He would also like to express his appreciation to Tuskegee Institute for granting permission to undertake the task.

ABSTRACT

The analysis, begun in an earlier grant, of the NASA data obtained on a VCHP heat-pipe radiator system which was tested in a vacuum environment was continued. The study included further analyses and interpretation of the steady-state results and an initial analysis of some of the transient data. Particular emphasis was placed on quanitative comparisons of the experimental data with computer model simulations. Although the results of the study provide a better understanding of the system which was experimentally investigated, they did not, unfortunately, provide a complete explanation for the major test anomolies, namely, the observed low VCHP performance and the relatively flat radiator panel temperature distribution. The results of the study also suggest, for future implementation, hardware, software, and testing improvements.

TABLE OF CONTENTS

LIST OF FIGURES

LIST OF TABLES

1.0 INTRODUCTION

As a result of L. B. Johnson Space Center sponsored feasibility heat-pipe radiator testing, valuable experimental data are being accumulated. In the study described herein, the analysis, interpretation and documentation of these data is continued. Particular emphasis has been placed on the use of computer thermal models.

An earlier study focused on the steady-state performance in the feasibility tests. Much of the data, however, were obtained under transient conditions. In the ultimate application of the systems envisioned, both transient and steady-state operating modes are important. Consequently, considerable emphasis was placed in the present study upon the transient results; and, in fact, distinguishing between steady-state and transient data. The latter effort was assisted greatly, but rather late in the contract period, by the computer program HPTRAN.

2.0 OPERATIONAL ANALYSIS OF FEASIBILITY VCHP

The purpose of this portion of the study was to isolate and examine phenomena pertinent to the operational characteristics of the feasibility VCHP. Particular attention is paid to its observed reduced maximum capacity. First, the complete feasibility VCHP results were examined, and certain data were selected, which seemed the most enlightening, for special study.

The control equation for a VCHP with a cold-wicked reservoir is:

$$\frac{L_{ca}}{L_c} = 1 + \left[\frac{V_R}{V_c} (P_V - P_{V_R}) / T_R - \frac{m_g R_g}{V_c} \right] \frac{T_s}{(P_V - P_{V_s})} \quad 2\text{-}1$$

Since V_R/V_c and $m_g R_g/V_c$ are fixed design parameters, then from Eq. (2-1), it can be seen that the active VCHP condenser length parameter Ψ depends upon P_V, T_R, and the inactive condenser length temperature T_s. It was shown in reference 1 that the effect of T_s on Ψ is small, so that Ψ is largely determined by P_V and T_R.

The vapor temperature T_V corresponding to P_V can be expressed by:

$$T_V = T_{mean} - Q_{REJ}/Cl$$

where T_{mean} refers to the mean temperature of the coolant as it flows through the heat exchanger. Thus, Ψ can either be

increased or decreased by changes in the inlet temperature T_{IN} of the coolant to the heat exchanger, the reservoir temperature T_R, and Cl. The conductance Cl depends upon the flow rate $\dot{m}$ of the coolant.

The above brief summary is not limited to any specific wick and is deduced from a study of the ψ equation, Eq. (2-1); which is theoretically derived and is believed to be valid. Previous analysis (1,2) of the operation of the VCHP in the feasibility tests have shown that under design conditions the experimental ψ values were less than theoretical when ψ was about 0.4 or higher, resulting in a serious reduction in the heat transport of the VCHP. In fact, at maximum design conditions the actual ψ reached a value only slightly over 0.6, considerably less than the expected fully-open value of 1.0. As a result, the effective area of the panel was only about one-half of its actual area.

2.1 Steady-State Evaluation

The VCHP parameters that best define the operation of a VCHP are the operating temperature T_V, the heat rejected, Q_{REJ}, the reservoir temperature T_R, and the environment temperature T_E, (or Q'_A). Useful operating curves for a VCHP can, therefore, be obtained by various plots using these parameters. Figures 2.1 and 2.2 taken from data used in reference 1, are examples, where T_V is plotted versus Q_{REJ} and ψ .

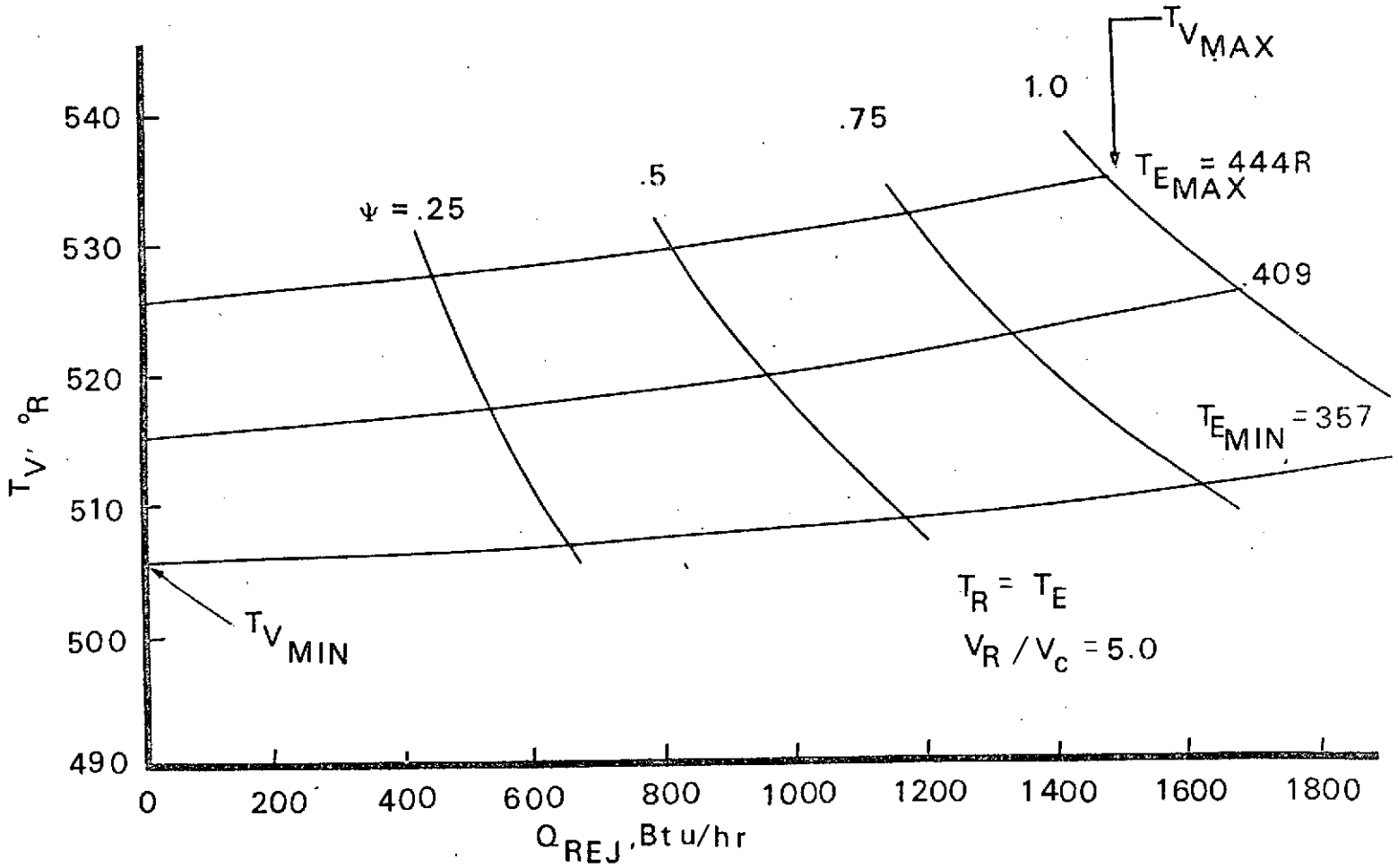

FIGURE 2.1 T_V vs. Q_{REJ}; $T_E = T_R$ and $V_R/V_c = 5.0$

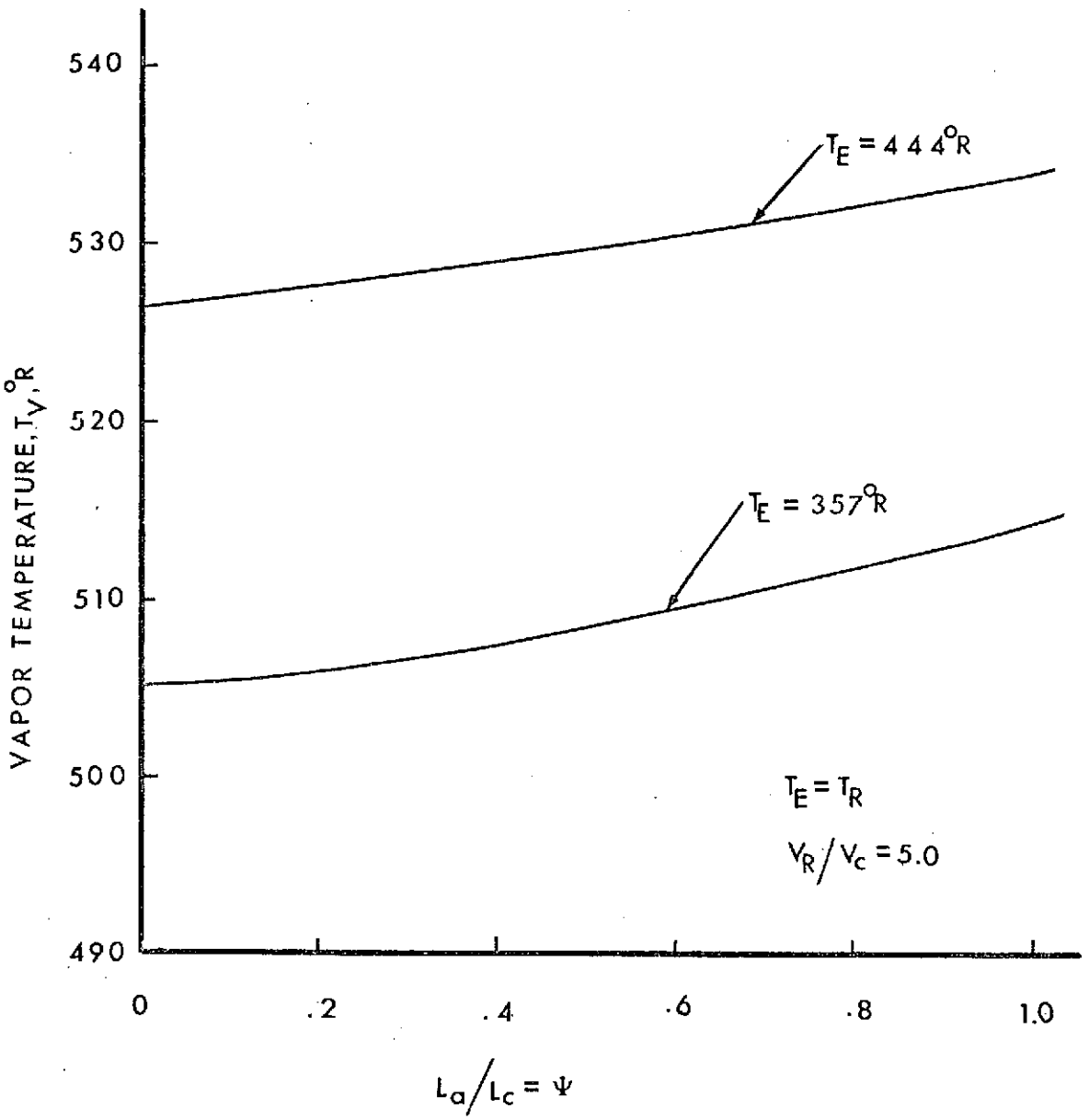

FIGURE 2.2 T_V vs. Ψ ; $T_E = T_R$ and $V_R/V_c = 5.0$

Lines of constant T_E, (T_R assumed equal to T_E), are also included in the diagrams. The data presented are analytical values and were obtained from the steady-state heat-pipe radiator system computer program PRFORM (3). The principal characteristic of these curves is that for a given environment the increase in operating or vapor temperature of the VCHP is small ($\approx 8^{\circ}$) as the ammonia vapor - N_2 gas front moves from the VCHP fully-off to the VCHP fully-on positions. In addition to this small temperature rise, it can be observed that between the two limiting positions there is nearly a straight-line variation in vapor temperature. Therefore, a good indication of the operation, and control, of a VCHP during a test can be established from a plot of the VCHP vapor temperature versus the front location when compared with theoretical predictions. Unfortunately, in reality, the front is not flat, and its position cannot be measured directly. In addition, the vapor temperature is not normally measured due to sensor installation complications. The front location can be estimated from the axial outside surface temperature measurements along the VCHP condenser. The vapor temperature should be approximately the same as the surface temperature measurement of the "low - k" section located between the VCHP evaporator and the VCHP condenser. Using those data as the best available approximations of T_V and

Ψ , an attempt was made to construct operating curves, Figs 2.3 and 2.4, for the VCHP used in the feasibility tests. It was desired that each data point in a particular sequence would have nearly equal environmental temperatures and nearly equal reservoir temperatures, which, in addition to the necessity of steady-state heat transfer, greatly reduced the number of data points that could be used from the feasibility experimental program. Consequently, a "minimum" of three data points could be found for only four test sequences. These were sequences 6, 7 (combined) and sequences 16, 17 (combined). The former was made with a low <u>design</u> environment, and the latter with a high <u>design</u> environment.

2.1.1 <u>Sequence 6, 7</u>

Referring to Fig. 2.3 and Table 2.1, as the inlet temperature to the heat exchanger was increased by a large increment, from 80 to 125 F, with T_E = -83 to -90F, and T_R = -83 to -86F, i.e., $T_R \approx T_E$, the vapor temperature, Fig. 2.4, and Ψ changed remarkably little, 61 to 62 F and 0.43 to 0.45, respectively. Theoretically, the VCHP should have been fully open, Ψ = 1.0, at an inlet temperature slightly above 90F. The theoretical VCHP opening temperature, Ψ = 0, for sequence 6, 7 conditions is about 47F. It was pointed out in reference 1 that the feasibility VCHP actually opened a few degrees lower than predicted. Thus, it can be

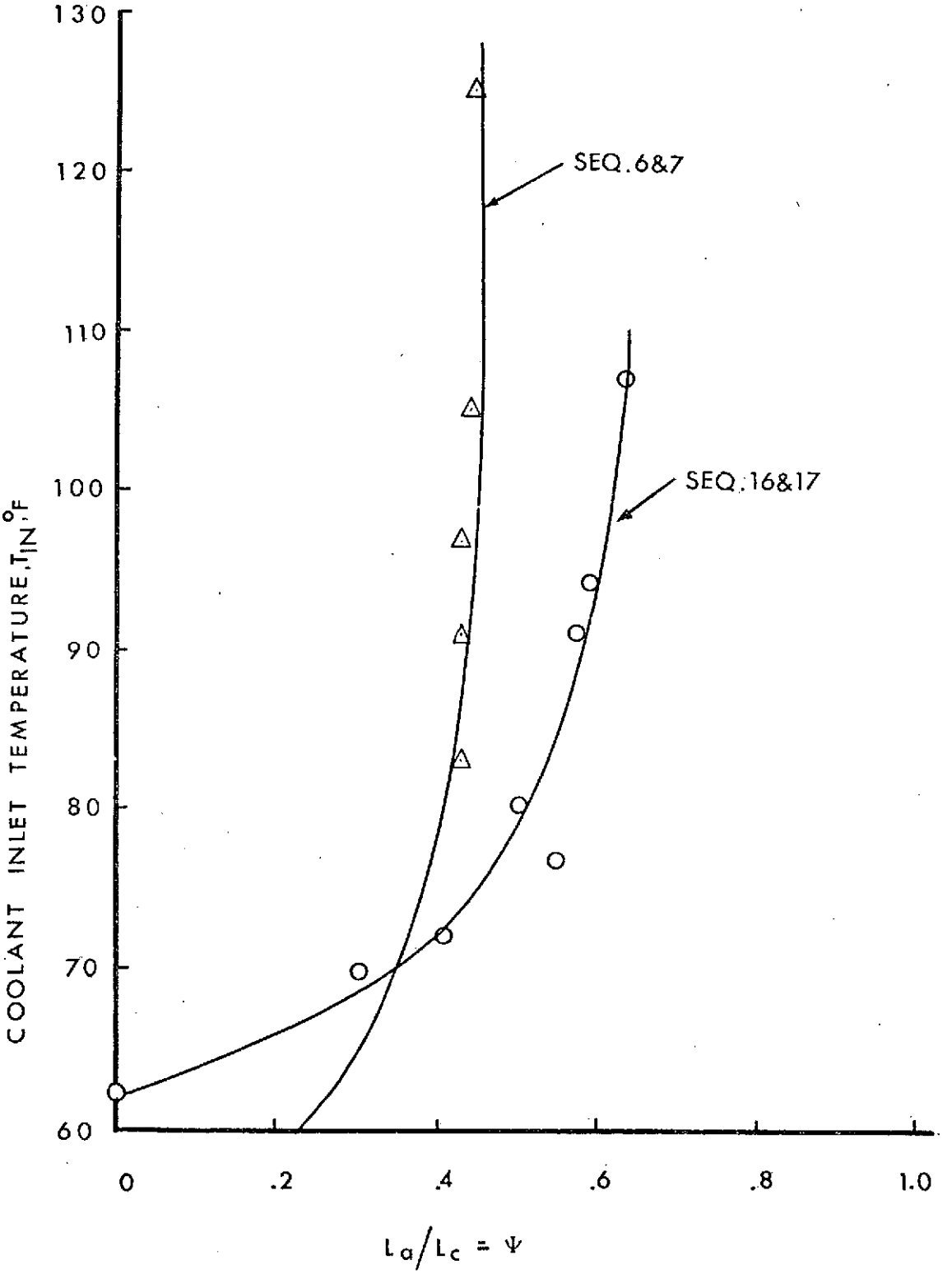

FIGURE 2.3 T_{IN} vs. Ψ ; Feasibility VCHP Data

Seq. No.	Run Time	Data Set No. (Ref. 4)	T_{IN}, °F	T_V, °F	Ψ
6,7	191-17-36	13	83	61	.43
6,7	191-18-05	15	91	61	.43
6,7	191-18-45	15	97	61	.43
6,7	191-19-13	17	105	62	.45
6,7	191-19-33	17	125	62	.45
16,17	192-07-51	30	70	70	.32
16,17	192-10-50	34	72	68.5	.36
16,17	193-08-30	54	72	71	.42
16,17	192-23-25	39	77	76	.56
16,17	192-07-31	30	80	79	.51
16,17	192-06-45	30	91	79	.58
16,17	192-07-06	30	94	80	.6
16,17	194-07-20	73	107	86	.65

TABLE 2.1 Feasibility VCHP data

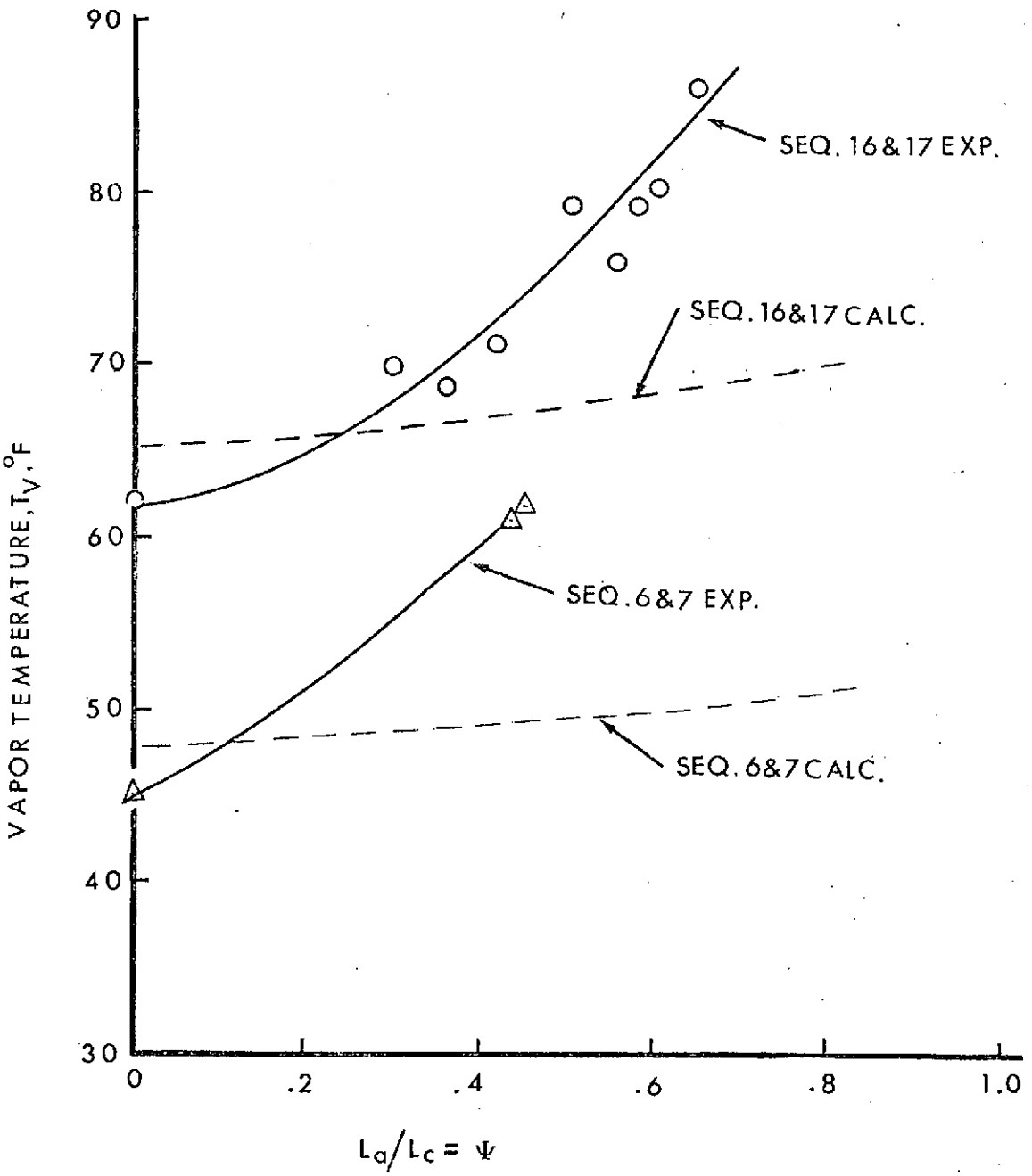

FIGURE 2.4 T_V vs. Ψ ; Feasibility $\overline{\text{VCHP}}$ Data

concluded that the cross-over point for the VCHP was between an inlet temperature less than 47F and the next experimental point at 80F and Ψ between 0 and 0.4. The cross-over point is where the experimental T_V became higher than theoretical. With an environment temperature of -83 to -90F, although the data are not complete, it can be deduced that the feasibility VCHP began to malfunction probably before it was 1/4 open. The large increase of T_V with T_{IN} is typical of a wick that is in the process of drying-out, and in this case, prematurely.

2.1.2 Sequence 16, 17

Referring to Fig. 2.3 and Table 2.1, as the inlet temperature to the heat exchanger was increased from 70 to 72F, T_E = -13 to -20F and T_R = -13 to -19F, i.e. $T_R \approx T_E$, the vapor temperature, Fig. 2.4, increased only slightly, and Ψ increased appreciably, from 0.32 to 0.42, indicating good VCHP control. As T_{IN} was increased further to 107F, however, the vapor temperature rose sharply to a value of 86F with Ψ not exceeding 0.63. The VCHP opened at about 62F. Thus, the cross-over point for the VCHP was between 62 and 71F. With an environment of -13F to -20F, the data indicate that the feasibility VCHP was probably operating reasonably close to expectations up to an inlet temperature of 70F, or until the VCHP was about 2/5 open. This was some

improvement over sequence 6,7 but above 70°F again the large increase of T_V with T_{IN} is typical of a wick that is drying out.

2.1.3 Heat Transport Q_{REJ}, Watts and $Q_{REJ} \cdot L_{eff}$, Watt-inches

In reference 1, the heat rejection capacity of the feasibility VCHP was represented by the parameter Q_{REJ}. A better parameter for expressing the heat transport of a heat pipe is the parameter $Q_{REJ} \cdot L_{eff}$, where L_{eff} is the effective transport length and is determined for the feasibility VCHP from:

$$L_{eff} = \tfrac{1}{2} L_c + \tfrac{1}{2} L_{ev}$$

$Q_{REJ} \cdot L_{eff}$ was calculated from the feasibility steady-state data, and the highest values from the available data for the various sequences are presented in Table 2.2. Also presented are the Q_{REJ} values. It is interesting, and of possible significance, that Q_{REJ} is approximately the same for each sequence, but $Q_{REJ} \cdot L_{eff}$ increased as the environment temperature became larger. The implication here is that the VCHP watt-in transport capacity improved at the higher environments and operating temperatures. At the highest environment temperature, which was off-design, the VCHP performance apparently exceeded theoretical, due to higher than expected panel fin temperatures, (See Section 4.0.) At the maximum design

SEQ. NO.	RUN TIME	$\dot{m}$ lb/hr	T_{IN} ^{o}F	T_V ^{o}F	T_E ^{o}F	Q'_A $\frac{Btu}{hr\text{-}ft^2}$	Ψ	Q_{REJ} $\frac{Btu}{hr}$	$Q_{REJ} \cdot L_{eff}$ Watt-in.
6,7	191-19-13	290	105	62	-85	22	.48	1306	9,219
15	192-15-30	300	106.5	84	-11	58	.62	1293	10,496
16	192-17-35	1133	90	85	-7	59	.63	1256	10,251
17	193-01-10	2090	96	87	- 8	60	.66	1311	11,009
20	192-12-00	2000	120	114	50	93	.72		
20	193-11-15	1990	109	108	45	93	.78	1250	11,563
21	193-15-18	2000	139	139	105	138	.72	1321	13,161

TABLE 2.2 Q_{REJ} and $Q_{REJ} \cdot L_{eff}$ Results for the Feasibility VCHP.

environment, sequence 17, the VCHP maximum capacity was much less than theoretical.

2.2 Transient Evaluation

It is the intent now to point out, and investigate in depth, selected transient data that are believed to characterize the VCHP operation during the feasibility tests, and hopefully shed some additional light on its sub-performance. Equation (2-1), and the summary presented above, provide the theoretical background needed for the study.

2.2.1 T_{IN} Transients

As previously discussed, and also in reference (1), the inlet temperature, T_{IN}, of the coolant at the heat exchanger entrance has a strong influence on T_V and consequently on Ψ. Thus, the correct measurement of T_{IN} is important if the data are to be compared with analytical predictions. In the feasibility tests the inlet temperature was measured with an immersion thermocouple installed just upstream of the entrance to the heat exchanger. This measurement was designated AJ0020, Main Tube Inlet. In addition, a surface measurement, EN 001, was made on the inlet tube to the heat exchanger. Although AJ0020 should have provided the more accurate value of T_{IN} and has been used herein as such, there were periods during the test that EN 001 was apparently giving a better transient record of T_{IN}, if the

recorded data are valid. For example, refer to the experimental data for time period 192-06-06 to 192-06-14, Fig. 2.5 and 193-03-00 to 193-04-54, Figs. 2.6 and 2.7. In all of these periods, fluctuations of the VCHP temperatures can be seen which cannot be explained by reading AJ0020, since it remained fairly constant. The VCHP temperature traces, however, correlate very well with the recorded fluctuations of EN 001. If these data are valid, some doubt is cast on the use of AJ0020 for the coolant inlet temperature, particularly under transient conditions.

Early in the test series (191-15-08), the feasibility VCHP was inadvertently subjected to a near step change of T_{IN} of relatively large magnitude, Fig. 2.8. In about two minutes T_{IN} was increased from a value of 55°F to 140°F and then after two minutes was decreased to 130°F. In addition, as the inlet temperature increased, the flow rate also went up from 200 lb/hr to 700 lb/hr for two minutes and then was returned to its initial value. The effect of the change in coolant flow rate is discussed below. Thus, the VCHP was subjected to an extreme thermal shock, which resulted in some interesting and unusual transient behavior. Because of the fast thermal response of the heat exchanger, when the inlet temperature was increased at 191-15-08 the vapor temperature, sometimes called the VCHP operating temperature, rose

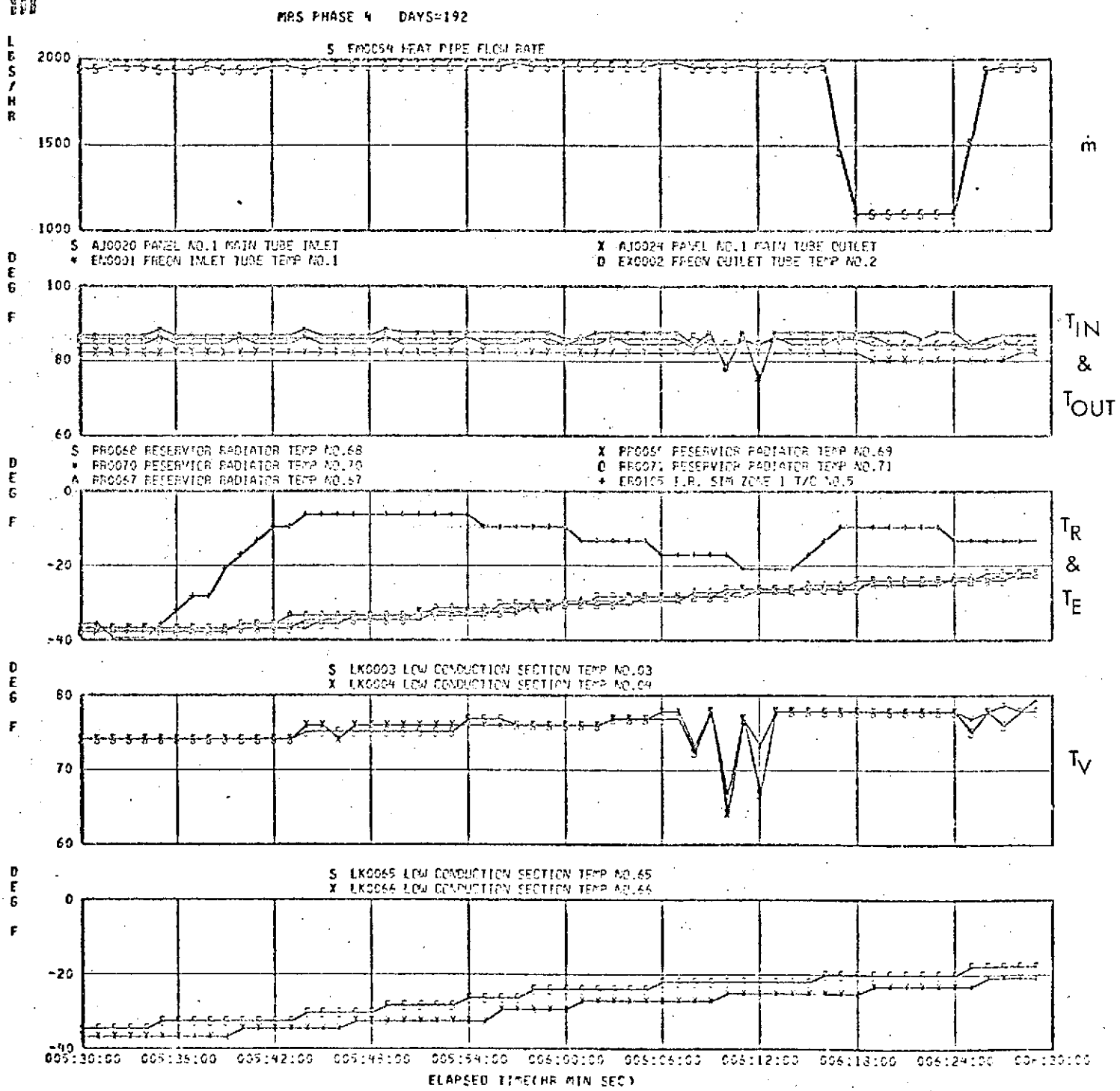

T = 192/05/30 - 192/06/29

Set 29

FIGURE 2.5 Experimental Feasibility Data for Time Periods 192-06-06 to 192-06-14

ORIGINAL PAGE IS
OF POOR QUALITY

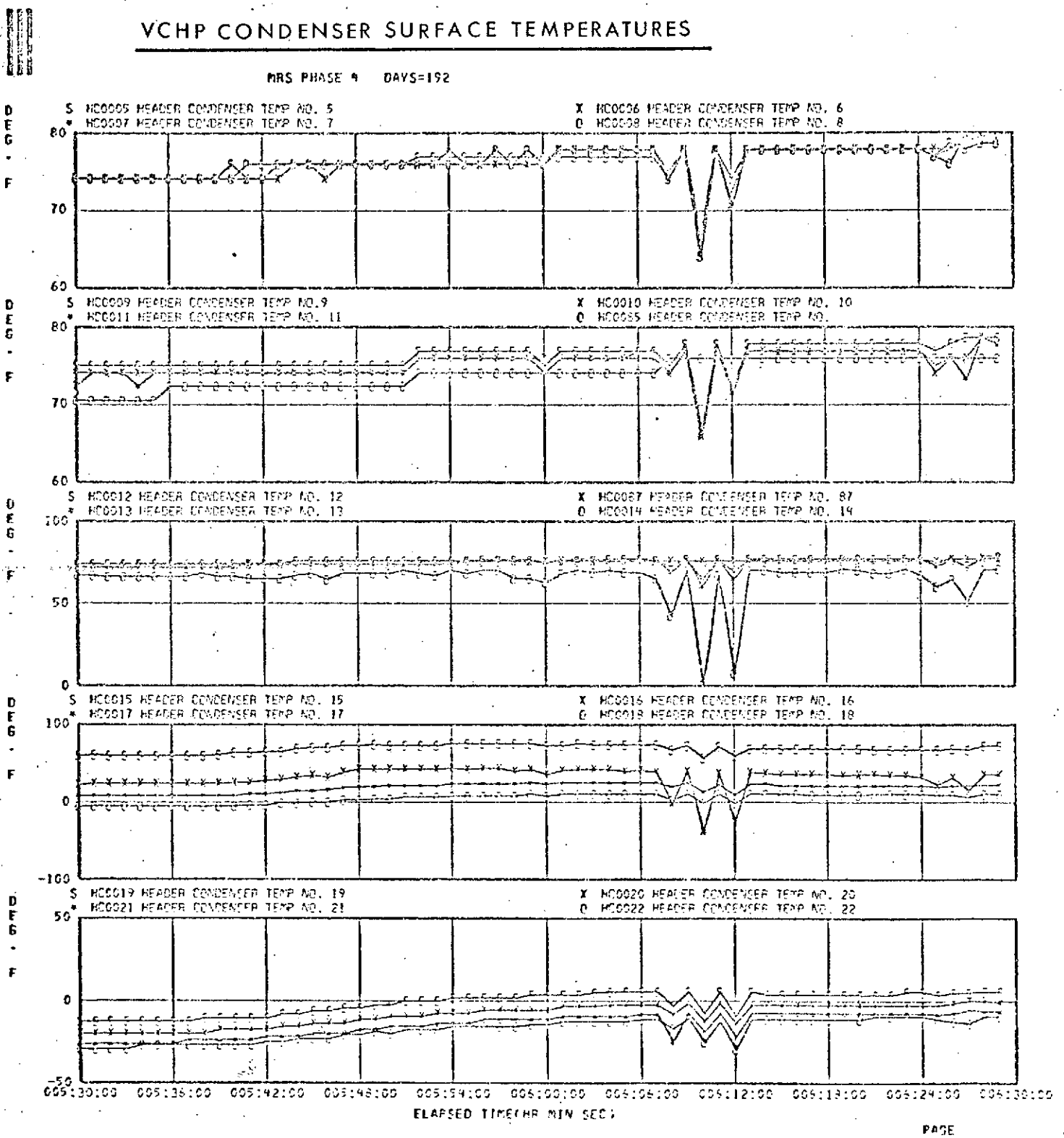

T = 192/05/30 - 192/06/29

Set 29

FIGURE 2.5 (con't.) Experimental Feasibility Data for Time Periods 192-06-06 to 192-06-14

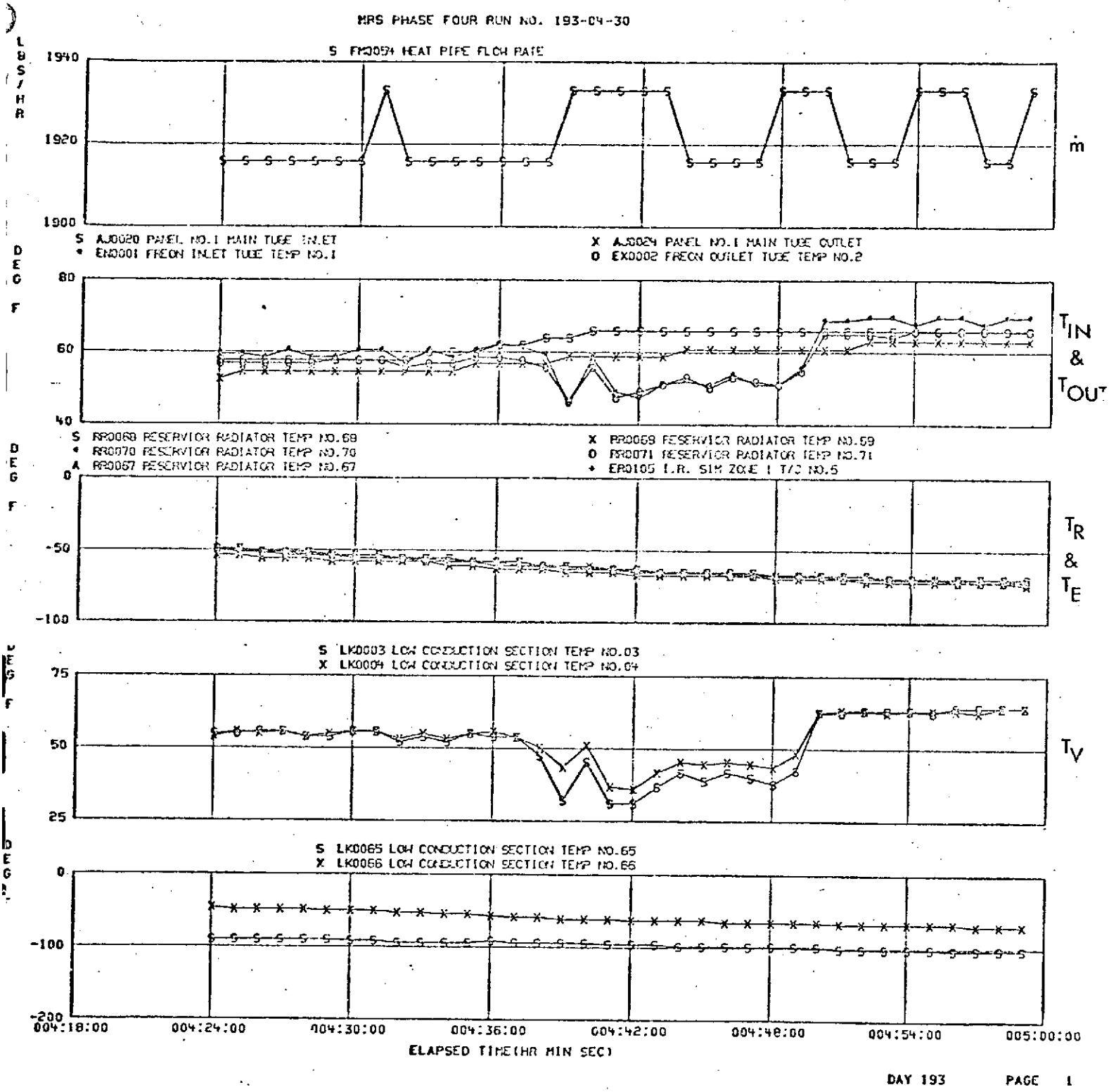

T = 193/04/24 - 193/04/59

Set 50

FIGURE 2.6 Experimental Feasibility Data for Time Period 192-04-12 to 193-04-59

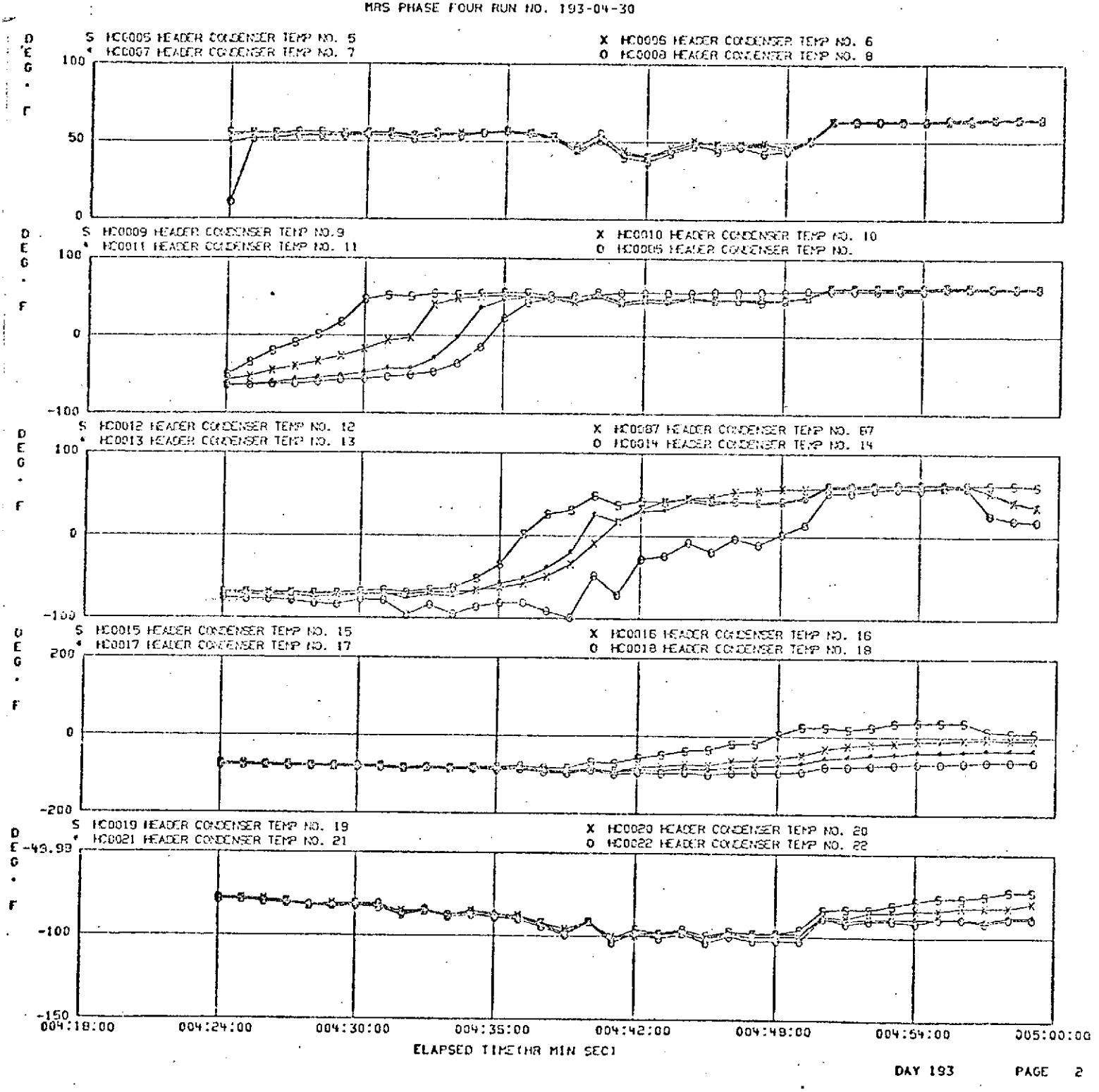

T = 193/04/24 - 193/04/59

Set 50

FIGURE 2.6 (con't.) Experimental Feasibility Data for Time Periods 193-04-12 to 193-04-59

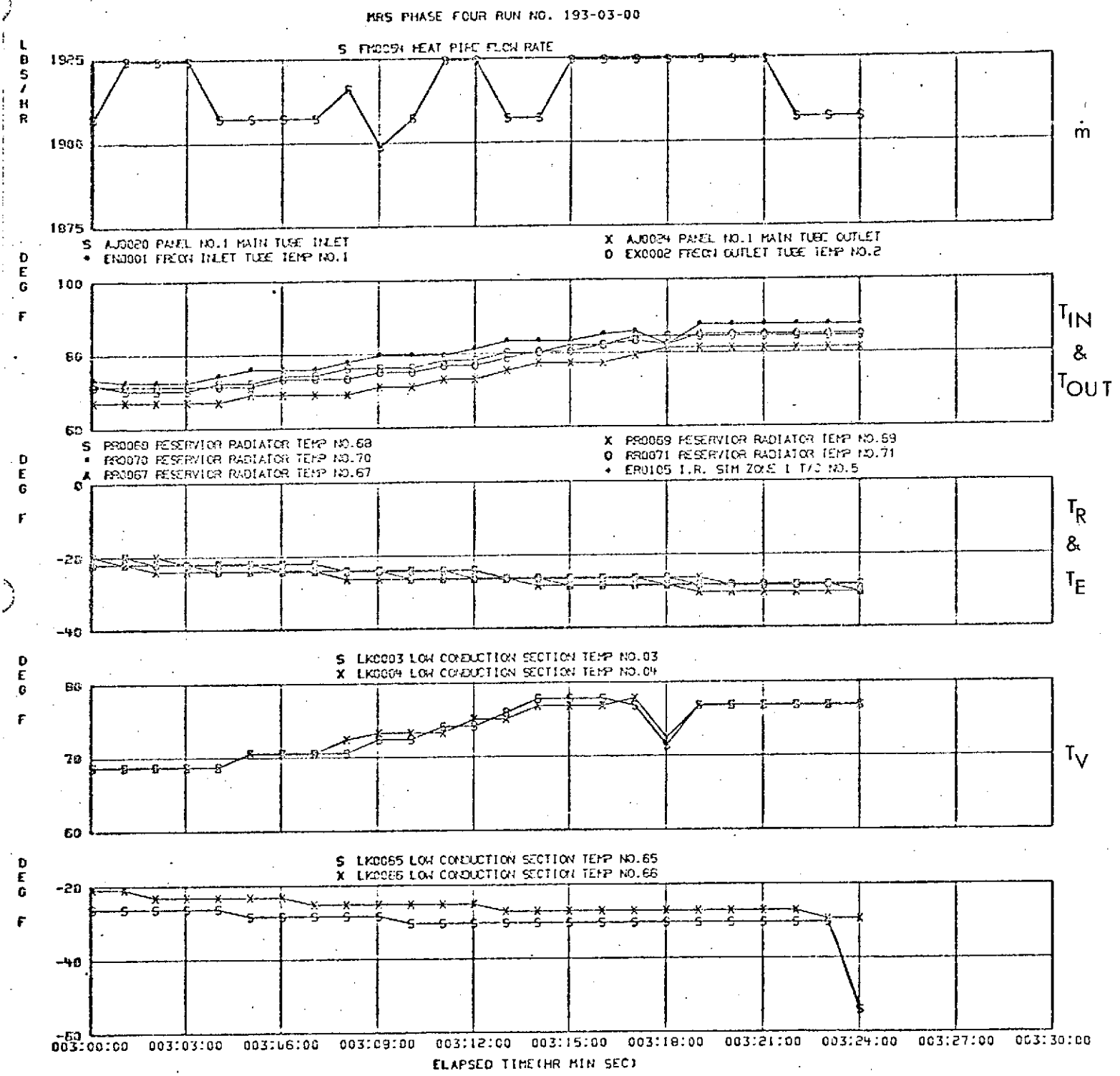

T = 193/03/00 - 193/03/24

Set 47

FIGURE 2.7 Experimental Feasibility Data for Time Period 193-03-00 to 193-03-24

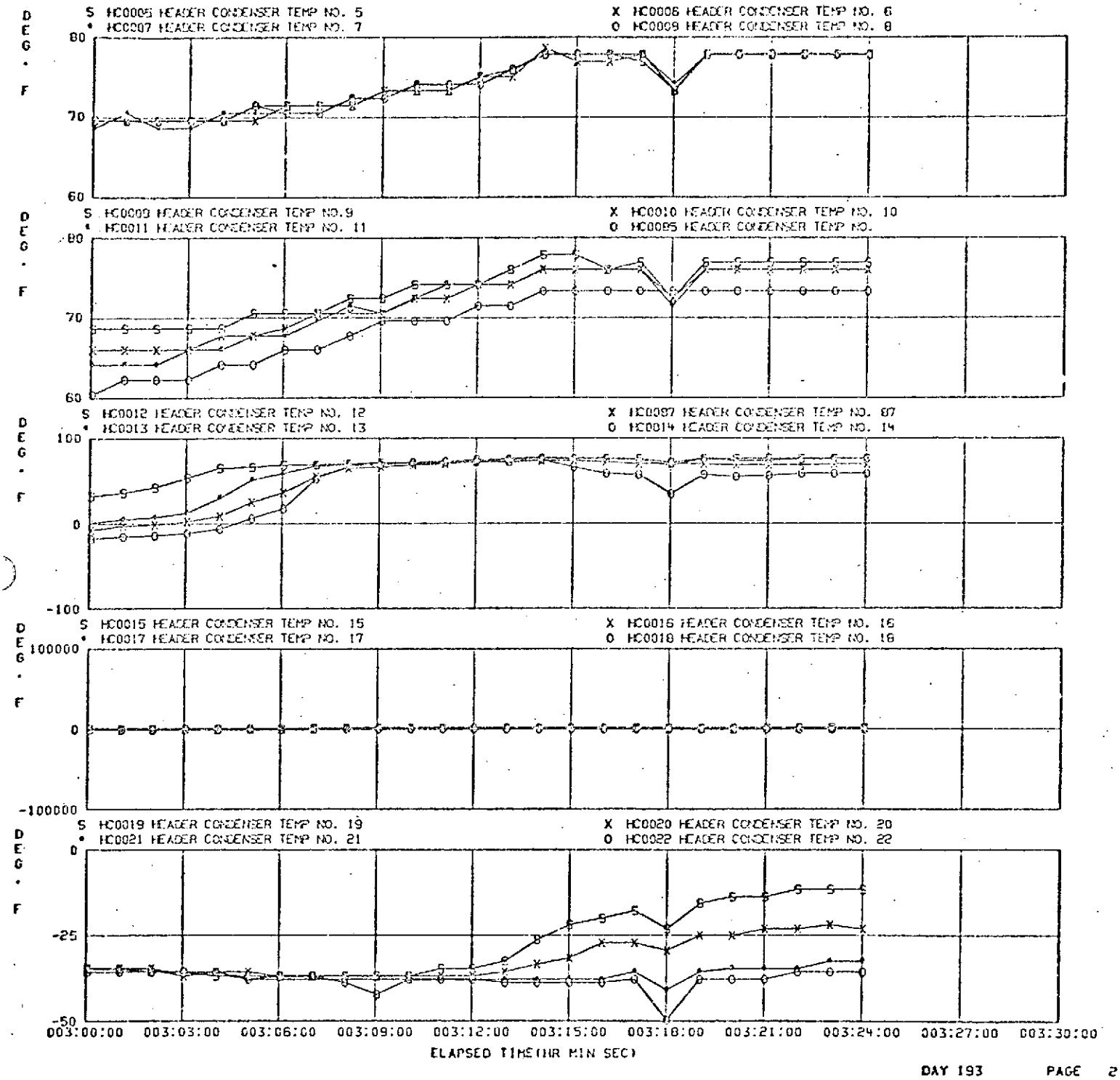

T = 193/03/00 - 193/03/24

Set 47

FIGURE 2.7 (con't.) Experimental Feasibility Data for Time Periods 193-03-00 to 193-03-24

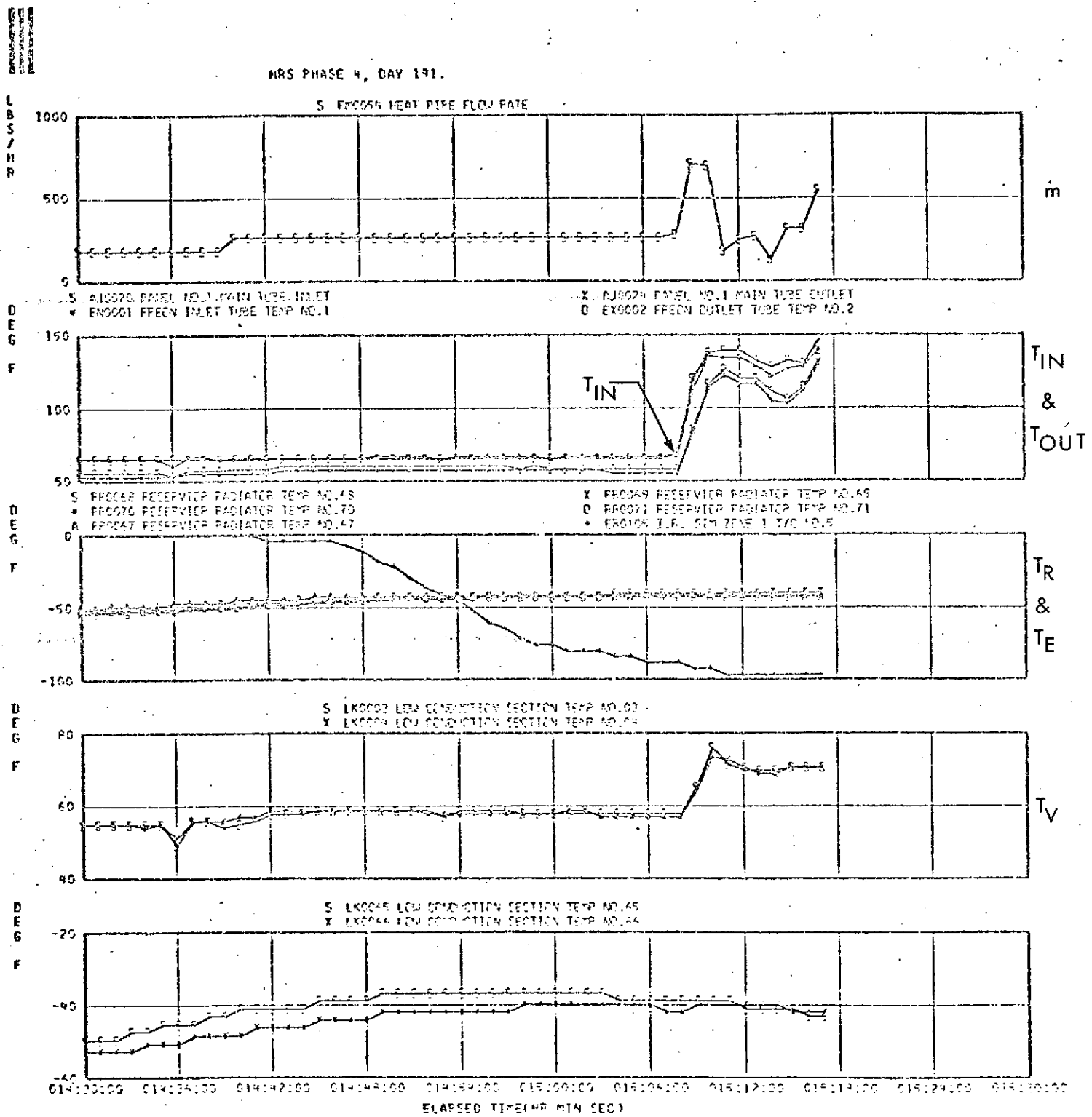

T = 191/14/30 - 191/15/17

Set 11

FIGURE 2.8 Large Rapid Increase of T_{IN}

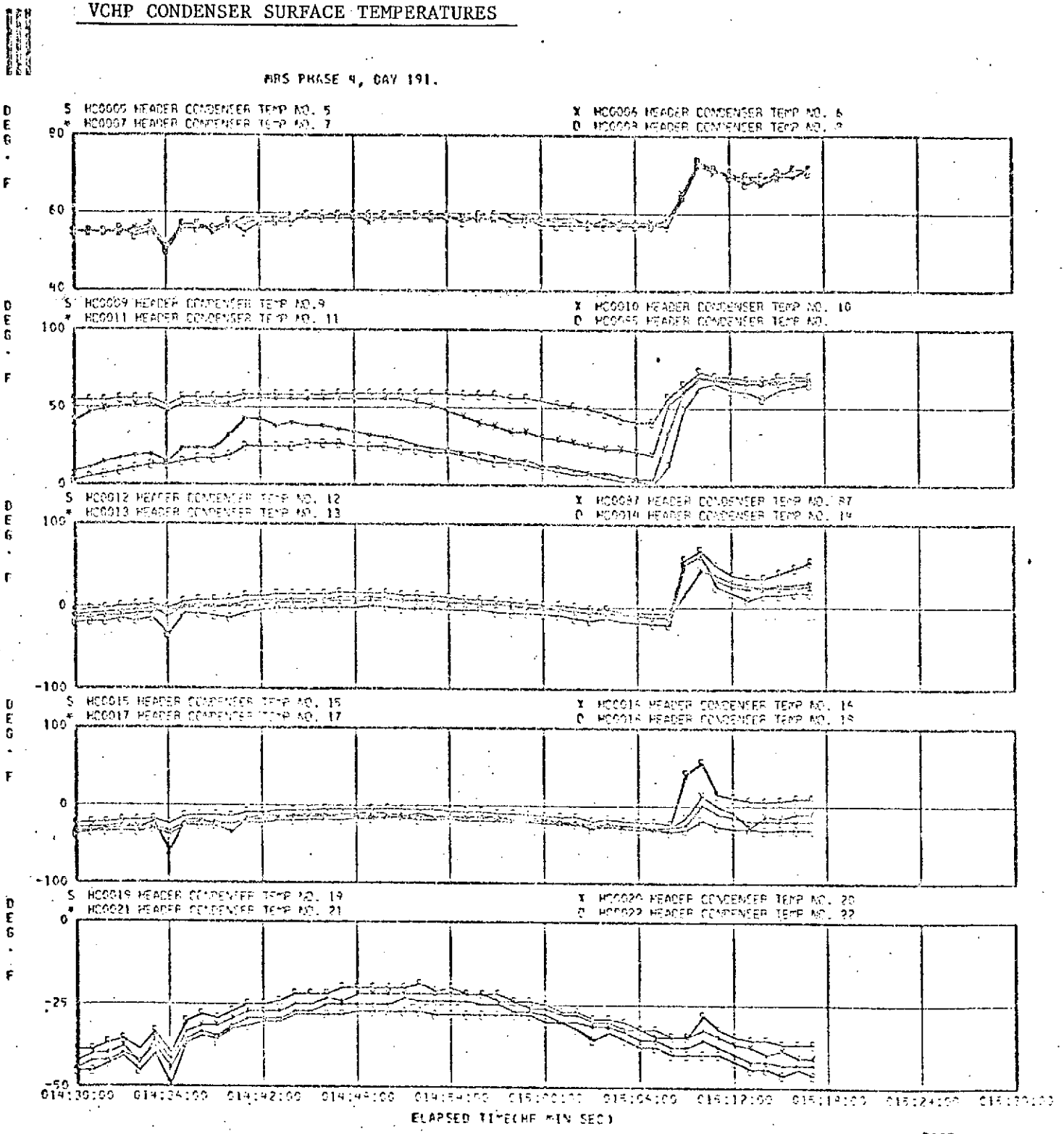

ΔT = 191/14/30 - 191/15/17

Set 11

FIGURE 2.8 (con't.) Large Rapid Increase of T_{IN}

at nearly the same rate reaching a maximum value of 75F and then dropping to 70F when the flow rate was decreased. The data seemed to indicate that if the flow had not been reduced Ψ would have reached a value of 0.6 in about 4 minutes. As it was, Ψ achieved a value of 0.55 in about 3 minutes. It is interesting to note that of the six feeder heat pipes feeder C was most sensitive (indicating lowest capacitance?) to the sudden thermal load applied to the panel. The VCHP responded quite rapidly to the thermal shock, but it only opened about half-way, even though T_{IN} was held between 125F to 150F for 11 minutes. This was certainly positive evidence early in the test program that the feasibility VCHP was not operating in the manner intended.

Start-up of the feasibility VCHP by increasing T_{IN} was discussed in detail in reference 1 and also in Section 3.0 of the present report. During shutdown the movement of the vapor-gas interface is toward the evaporator and the transients that occur are again of interest. An example of the shutdown of the VCHP by decreasing T_{IN} is presented in Fig. 2.9 where data are presented for the time period 192-17-50 to 192-18-25. At the beginning the VCHP is open with $\Psi \approx 0.6$, $T_{IN} = 100F$, $T_R = -8F$, $Q_A' = 60$ Btu/hr - ft^2 and $\dot{m} = 1200$ lb/hr. During shutdown $\dot{m}$ increased to 1900 lb/hr but this change had negligible effect on the shutdown. (See

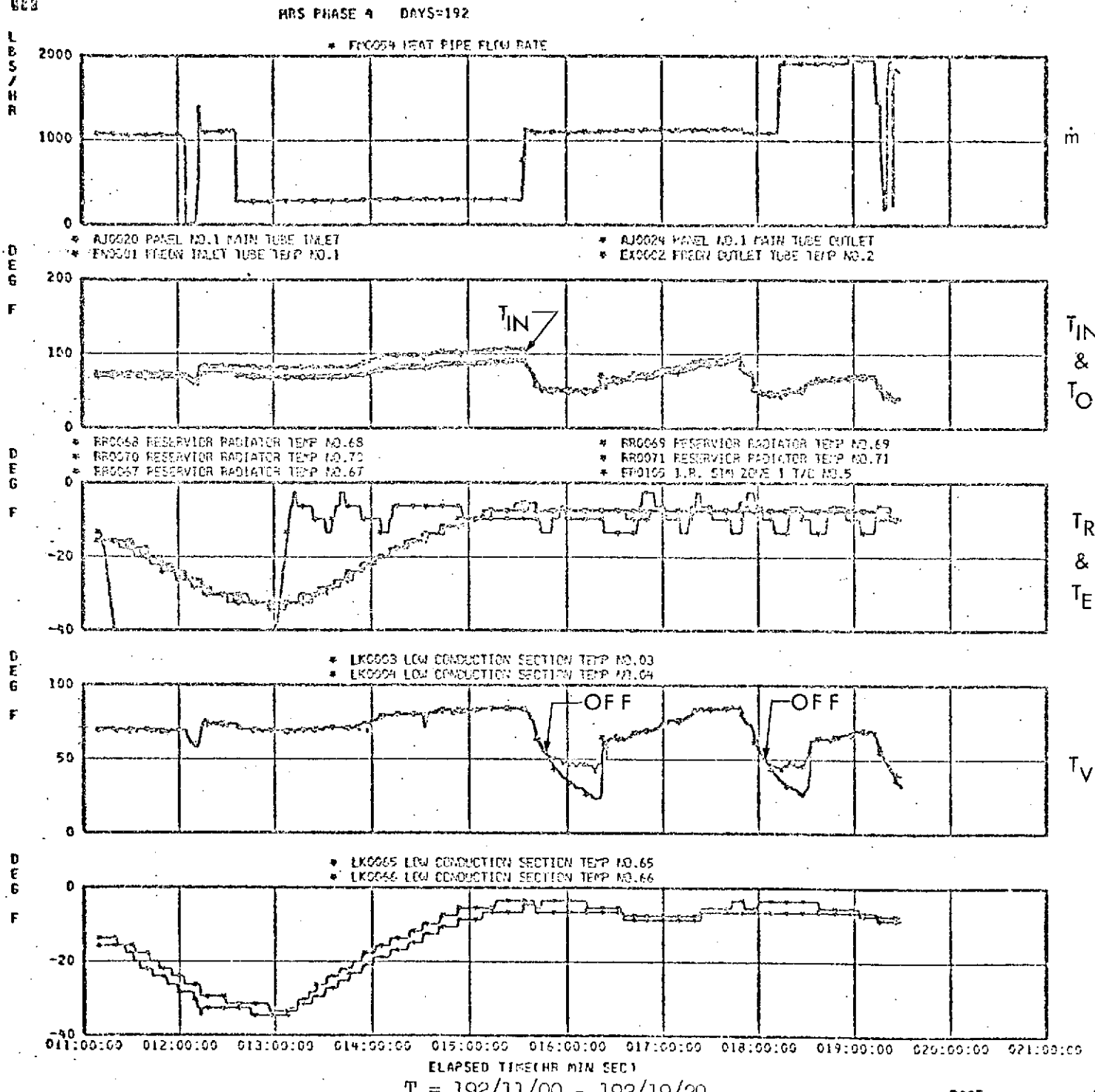

Set 35

FIGURE 2.9 Shutdown of Feasibility VCHP by Lowering T_{IN}

VCHP CONDENSER SURFACE TEMPERATURES

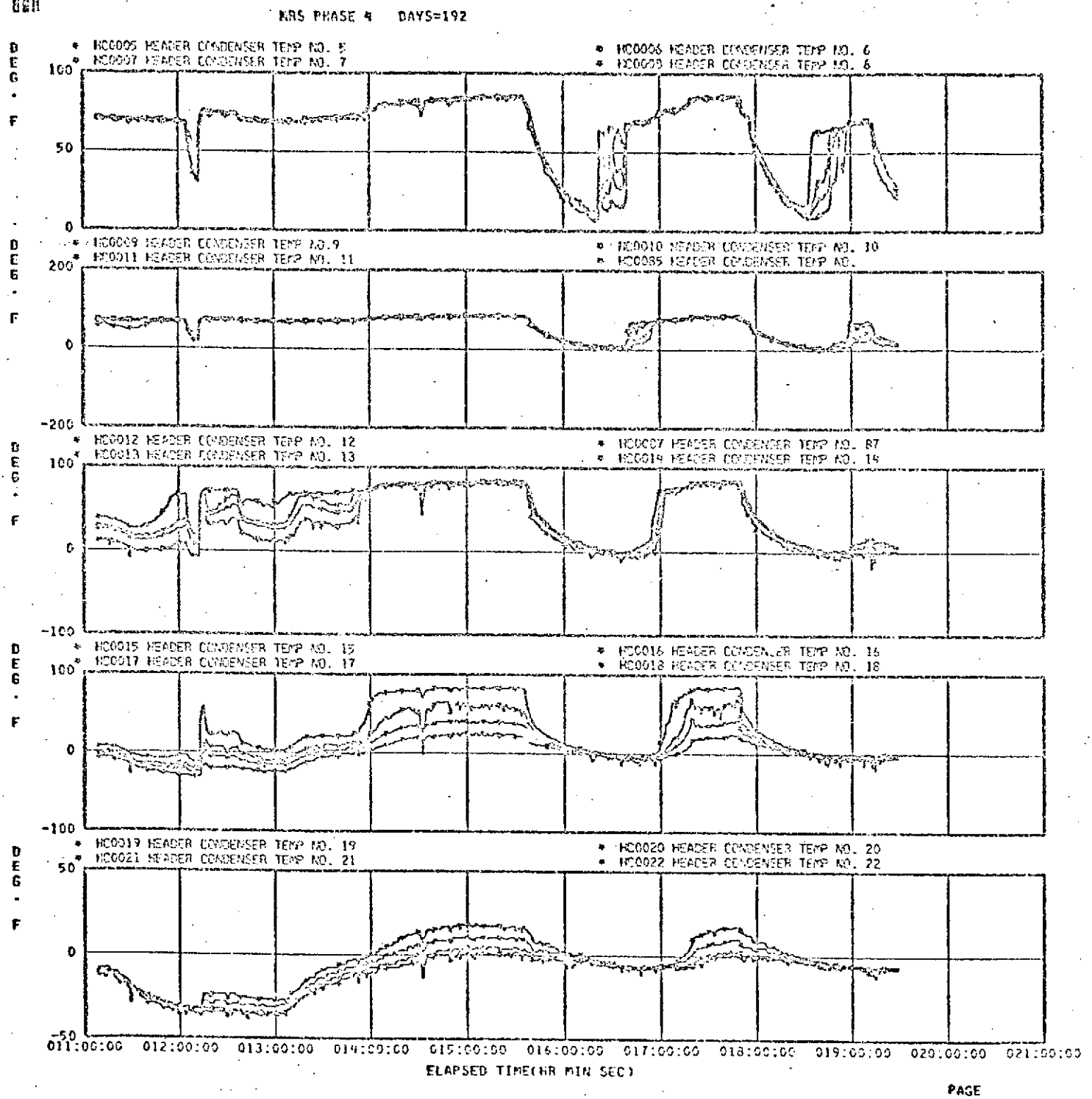

T = 192/11/00 - 192/19/29

Set 35

FIGURE 2.9 (con't.) Shutdown of Feasibility VCHP by Lowering T_{IN}

the effect of $\dot{m}$ on Ψ below). The inlet temperature was dropped from 100F to 75F in about 5 minutes, (which resulted in Ψ decreasing to slightly less than 0.5) held at 75F for about 5 minutes and then was decreased to 50F in about 5 minutes, followed by a final decrease to 45F, after approximately another additional 18 minutes. The VCHP closed, $\Psi = 0$, when T_{IN} became 45F.

2.2.2 T_R Transients

It was pointed out above that Ψ can be made to increase or decrease by variation of T_R, all other conditions remaining constant. When the feasibility VCHP was not at its maximum capacity the predicted effect of T_R on Ψ was qualitatively confirmed by the experimental results. Referring to the experimental data, for the time period 193-07-48 to 193-08-36, Fig. 2.10, an elapsed time of 48 minutes, it can be seen that the inlet temperature, T_{IN} and $\dot{m}$ are nearly constant at 71F and 1850 lb/hr., respectively. The reservoir temperature, however, in that period increased from -26F to -20F, or $\Delta T_R = 6F$. The observed change in Ψ was from 0.45 to about 0.4 or $\Delta\Psi = 0.05$. Although qualitatively correct, the observed value of $\Delta\Psi/\Delta T_R$ was considerably less than expected. The vapor temperature, TC 3, remained nearly constant during this period, which was as expected.

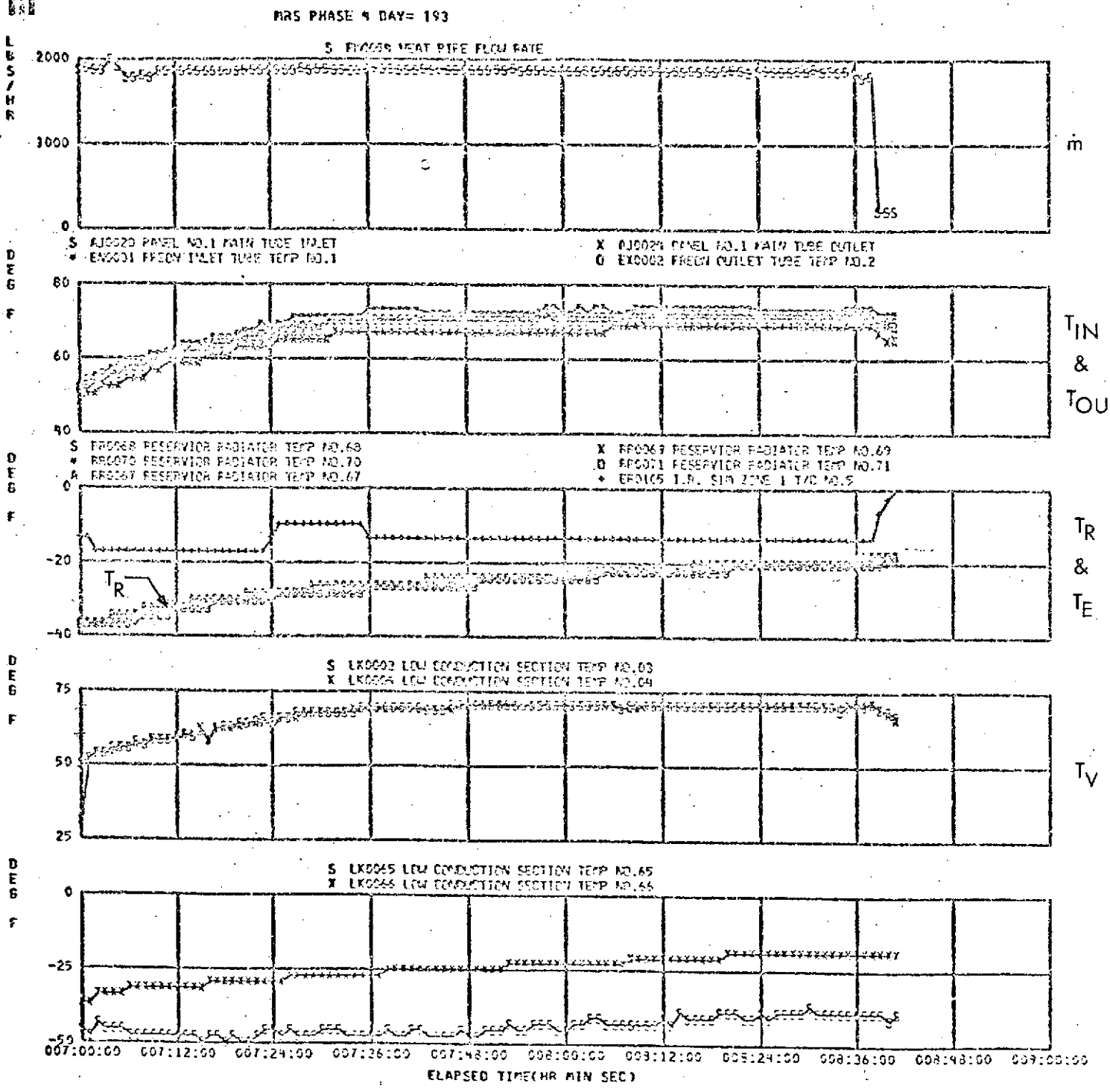

T_{IN} & T_{OUT}

T_R & T_E

T_V

T = 193/07/00 - 193/08/42

Set 53

FIGURE 2.10 Reducing Feasibility VCHP Capacitance by Increasing T_R

VCHP CONDENSER SURFACE TEMPERATURES

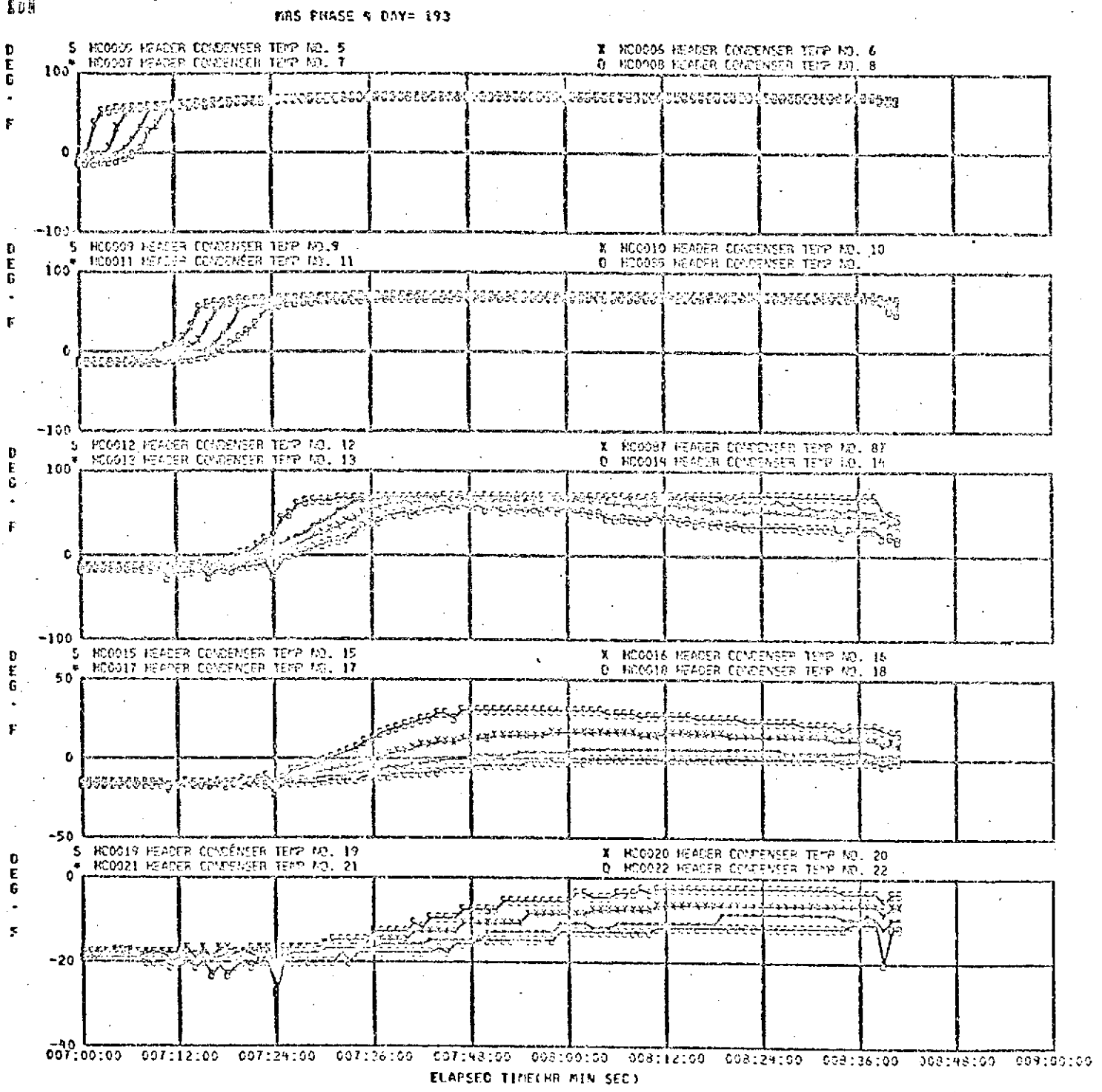

T = 193/07/00 - 193/08/12

FB

Set 53

FIGURE 2.10 (con't.) Reducing Feasibility VCHP Capacitance by Increasing T_R

Interesting VCHP operation occured between times 190-09-30 and 190-14-00, Fig. 2.11. In that period the VCHP was opened by the reservoir temperature decreasing while all other parameters were maintained constant.

Setting $\Psi = 0$ in Eq. (2-1), and from the experimental data, when $\Psi = 0$, $T_V = T_{IN} = 65^oF$, $T_s \simeq -50^oF$. For the feasibility VCHP, $V_R/V_C = 7.5$ and $m_g R_g/V_c = 1.8$. Using these data in Eq. (2-1), and solving for T_R gives -6.0F, which compares very well with the experimental value of $T_R \simeq -7.0^oF$.

After 190-14-00, the reservoir temperature continued to decrease, with T_{IN} and $\dot{m}$ constant, dropping to a value of -80.0^oF. At this point the observed Ψ value was about 0.3, much less than the corresponding calculated value of unity.

2.2.3 $\dot{m}$ Transients

Changes of the coolant flow rate may or may not affect the VCHP heat transport. For example, consider time 192-06-15, Fig. 2.5. The flow rate of the coolant was decreased from a value of 1950 lb/hr, the approximate design flow rate, to 1100 lb/hr at 192-06-18. During that change the reservoir temperature increased slightly, which would tend to decrease Ψ, but T_{IN} was constant at 84^oF. The major perturbation was the 50 per cent decrease in flow and it did not result in any decrease of T_V from its initial value of 78^oF or any detectable drop in the VCHP condenser temperatures. The latter implies that a 50 per cent reduction in the design coolant flow did not affect Ψ.

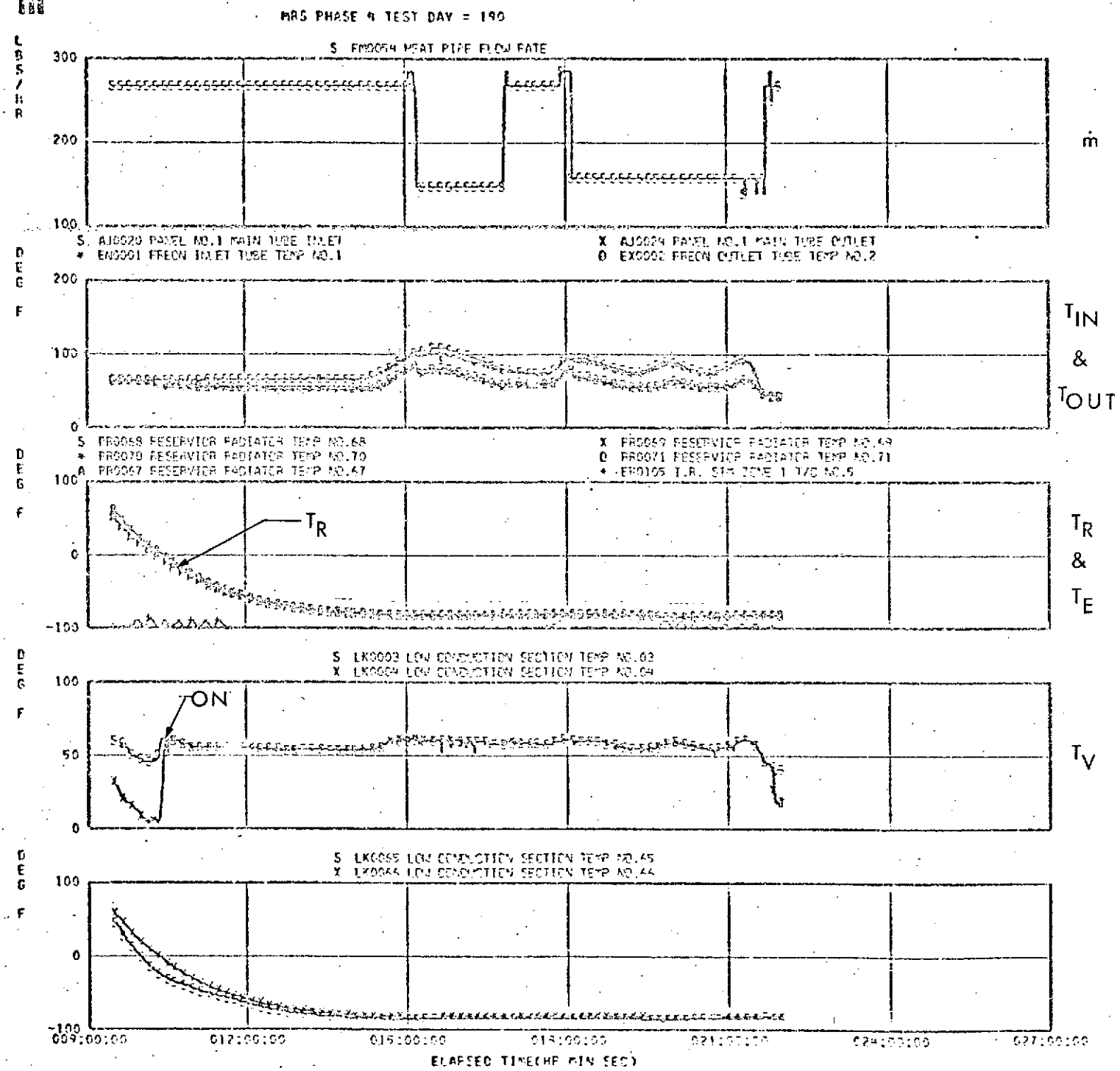

T = 190/09/30 - 190/22/00

Set 5

FIGURE 2.11 Turning-on Feasibility VCHP by Decreasing T_R

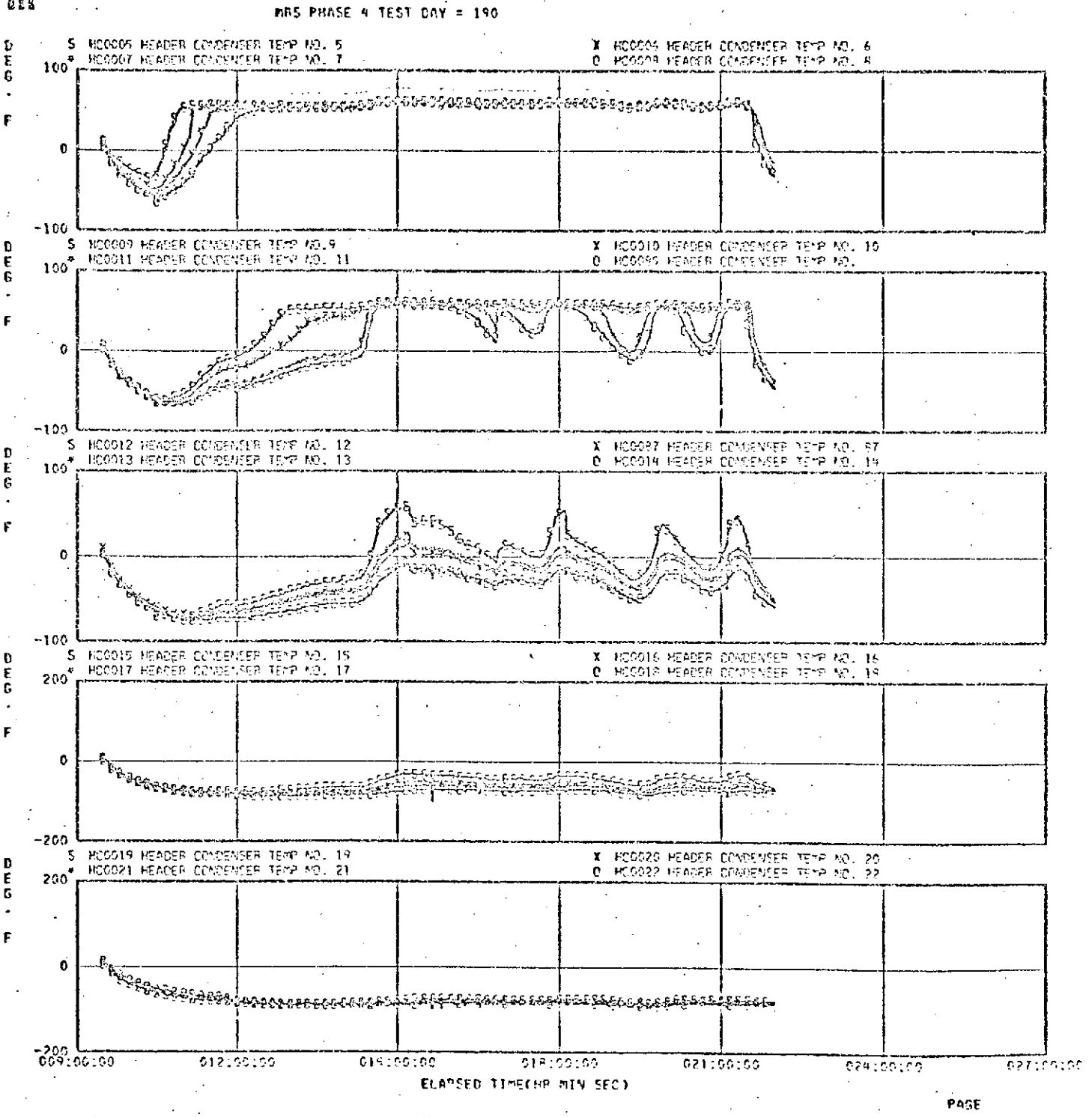

T = 190/09/30 - 190/22/00

Set 5

FIGURE 2.11 (con't.) Turning -on Feasibility VCHP by Decreasing T_R

On the other hand, the data of Fig. 2.8, which were used in the discussion above to illustrate the transients during a large, rapid increase of T_{IN} also provide an illustration where a decrease in $\dot{m}$ did affect the VCHP operation. At 191-15-10 the flow was lowered from 700 lb/hr to 200 lb/hr, which almost simultaneously lowered the vapor temperature from 75F to 73F, and Ψ from over 0.5 to between 0.4 and 0.45.

The data of 192-22-47, Fig. 2.12, illustrate the thermal response of the VCHP when the flow rate is rapidly and drastically reduced. From an initial value of 1840 lb/hr, $\dot{m}$ was reduced to below 400 lb/hr, and held at that level for two minutes. The flow was then momentarily shut-off before being brought back to its original value of 1840 lb/hr. This entire flow excursion took a little over ten minutes. During this period a significant drop in the readings from VCHP thermocouples nos. 5-13, that is, those surface thermocouples on the active portion of the VCHP before the flow was reduced, can be seen.

Consider now the data for time period 192-16-00 to 192-18-40, Fig. 2.9. During this time period the reservoir temperature was -8F and constant, and the VCHP was opened twice by increasing T_{IN}. The only apparent difference between the two was the magnitude of the coolant flow to the heat exchanger: 1150 lb/hr and 1875 lb/hr for the first and second start-ups, respectively. The lower flow-rate start-up began

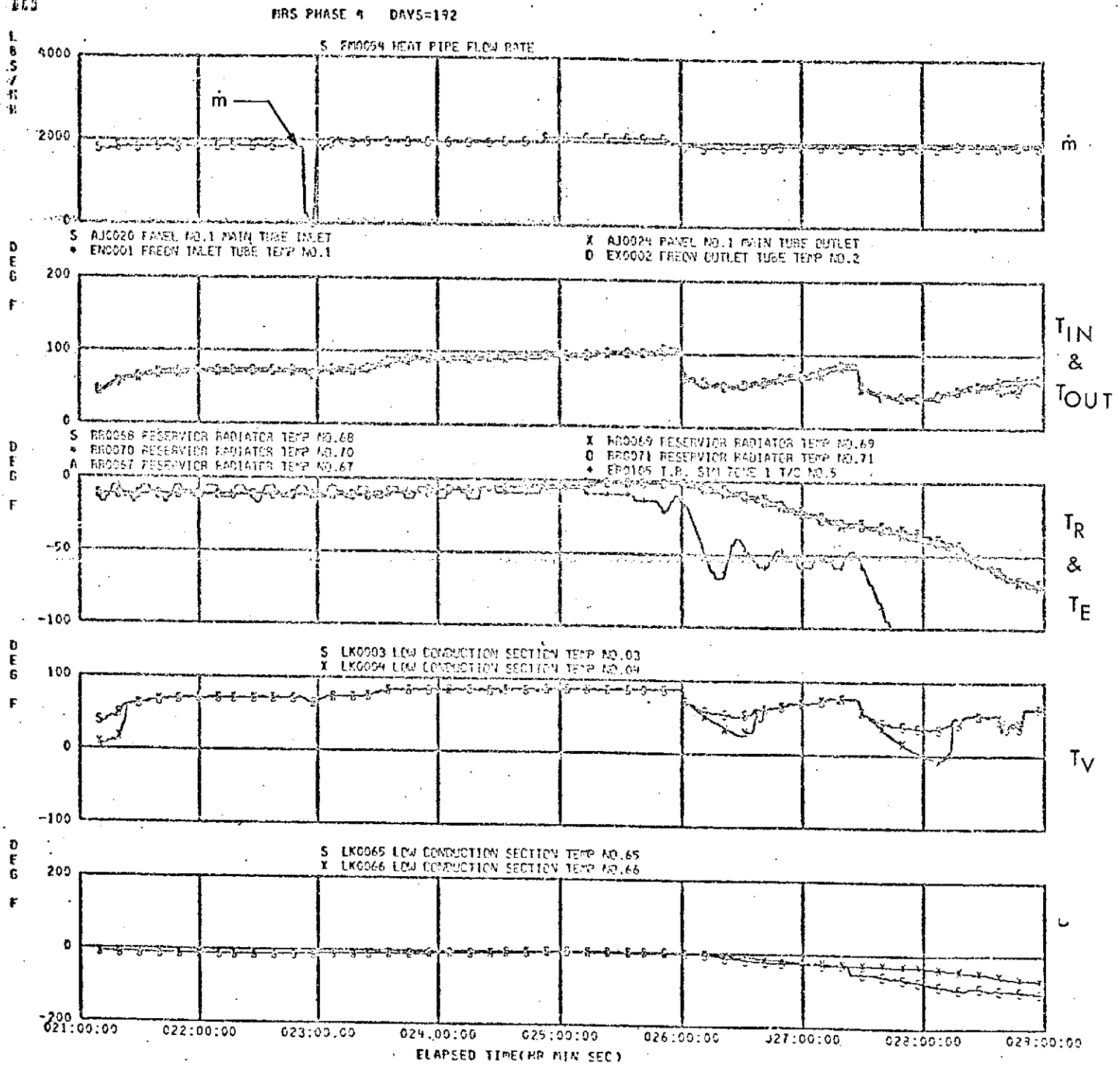

FIGURE 2.12 Effect of a Rapid and Large Drop of $\dot{m}$ on Feasibility VCHP

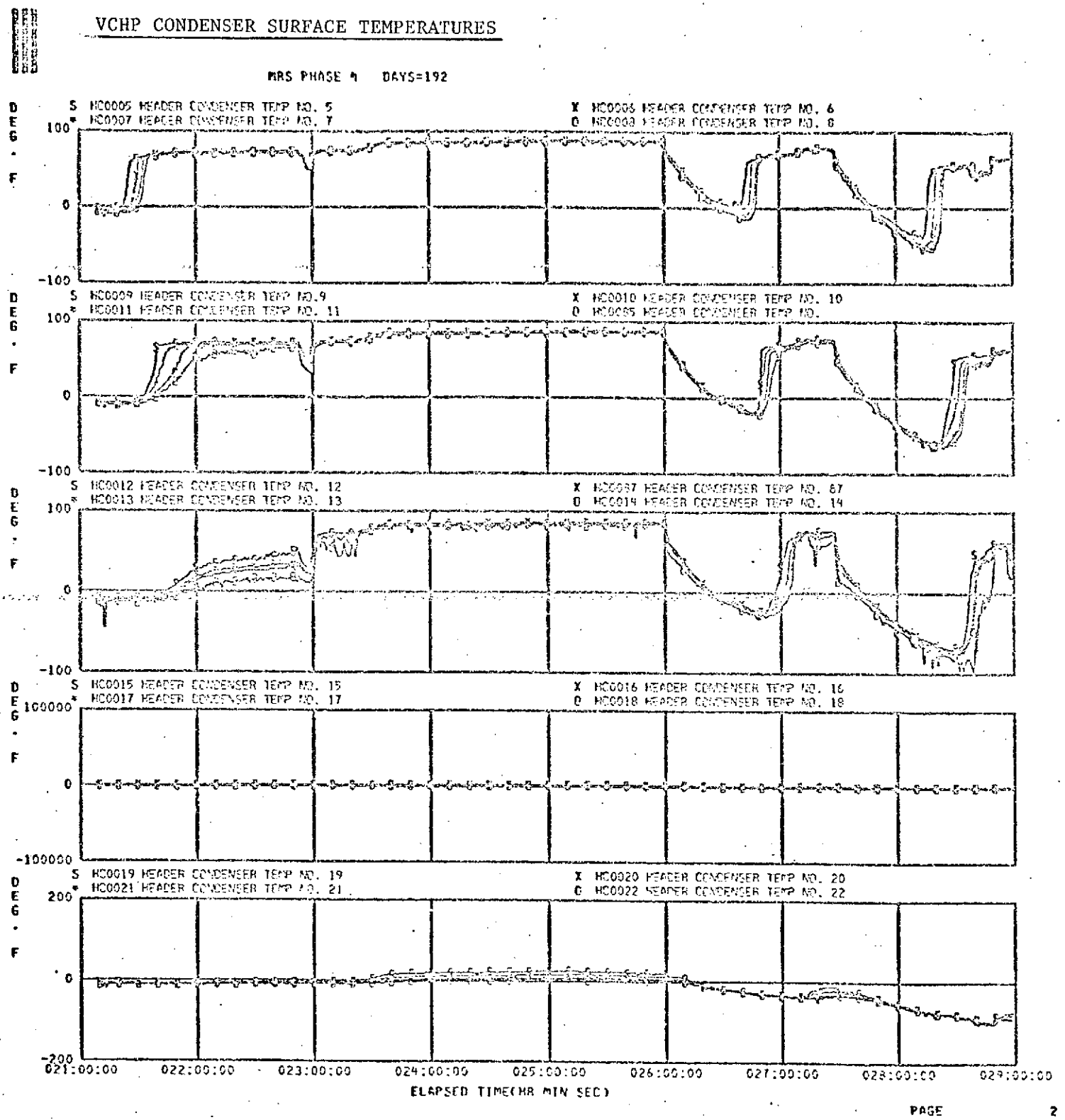

T = 192/21/00 - 193/05/00

Set 39

FIGURE 2.12 (con't.) Effect of a Rapid and Large Drop of $\dot{m}$ on Feasibility VCH

at a vapor temperature (equal to the inlet temperature) perhaps as much as 7^{o} lower than the start-up with the higher flow rate. It should be noted that in this sequence, as the inlet temperature was increased the VCHP condenser temperatures were decreasing at the point in time when the VCHP turned on.

3.0 LOCKHEEDS TRANSIENT HEAT PIPE HPTRAN PROGRAM

3.1 Need for a Transient Program and its Use in the Present Contract

Regardless of the particular type of radiator being considered for heat rejection, its ability to thermally respond within certain time limits to a change of operating conditions is an important characteristic of the system. It is not unreasonable to assume that during many duty cycles the heat rejection apparatus will be operating more frequently in a transient mode than in steady state.

A purported advantage to be gained by utilizing heat pipes in a heat-rejection system is a relative fast thermal response, but in order for the designer to make meaningful comparisons of candidate systems, the transient characteristics of each must be available and studied.

The feasibility heat-pipe radiator utilized a cold-wicked reservoir which, compared with wickless reservoirs, has a faster theoretical response, but again the lack of good quantitative data for each for comparison is evident.

There is a need for both experimental and analytical transient heat-pipe data, particularly under simulated operating conditions and obtained from experiments incorporating full-scale apparatus. The results obtained from the

feasibility heat-pipe system can be used as an excellent starting place toward fulfilling this particular need, specifically, for the case of a cold-wicked reservoir.

Although much data were taken over a wide range of operating conditions during the 102.3 hr. feasibility test program, the test variables were changed frequently throughout the test and it was often difficult to establish those times when steady-state had actually been achieved. Consequently, only about 10 steady-state points, Table 3.1, were listed in reference 1, an initial analysis of the test results made by the present author. With the aid of the transient computer program HPTRAN, (5), an objective under the present contract was to review and search the same data for additional steady-state points which, if successful, would permit a broader and more complete analysis of the results than was carried out in reference 1. Under the present contract this objective was not completely achieved for two reasons:

a. The transient computer program, HPTRAN, was not completed until late in the contract because of revisions. This greatly reduced the amount of available time for its use.

b. Programming difficulty was experienced converting the program to the computers available in the Tuskegee area.

TIME	SEQ.	T_{IN} F	$\dot{m}$ LB/HR	Q'_A BTU/HR FT^2	T_R F	ψ CALC.	Q_{REJ} CALC BTU/HR	Q_{REJ} PANEL TEMP BTU/HR	% DEV	Q_{REJ} ΔT BTU/HR
191-18-05	6,7	88.3	284	23	-84	.84	1770	1197	-30	1300
191-18-45	6,7	94.0	276	23	-85.5	1.0	1985	1217	-40	1310
191-21-40	14	71.0	276	41	-67	.5	887	945	+7	938
192-15-30	15	106.5	276	58	-7	1.0	1547	1293	-15	1240
192-10-50	16	71.0	1064	55	-16	.5	853	813	-2	855
193-08-30	17	71.0	1855	56	-19	.74	1238	980	-20	--
193-01-10	17	96.0	1990	60	-3	1.0	1825	1331	-30	--
193-10-20	20	90.0	1967	93	32	.51	608	795	+20	--
193-14-50	21	129.6	1985	137	93.5	.59	657	1058	+70	--
193-15-18	21	139	2000	137	102.0	.98	1147	1321	+20	--

Table 3.1 Steady-State Performance of Feasibility Heat Pipe Radiator System

3.2 Checkout of HPTRAN

Soon after the initiation of the present contract, Lockheed Electronic Corporation, Houston, Texas, at the request of NASA, began work on a transient heat-pipe radiator systems program. The program, which they named HPTRAN, (5), was an extension of their earlier steady-state program PRFORM.

Before HPTRAN could be used with confidence in the present investigation, however, it was necessary to make certain checks and to establish that the program gave reasonably valid results over the range of conditions of interest. The experimental data (4) obtained in the feasibility tests could be used in the comparisons and validation.

Most of the initial comparisons between HPTRAN results and the experimental data gave very poor agreement. It was not certain how much of the disagreement was due to the new transient additions to this program and how much was due to the fact that the position of the vapor-gas front in the VCHP condenser of the feasibility hardware did not agree with the analytical predictions (1,2). The latter discrepancy was known prior to the writing of HPTRAN and is due to the sub-performance of the VCHP.

It was clear that the only method of checking the transient portion of HPTRAN using the feasibility test data was to input into the program the experimental front position

versus time. Unfortunately, the actual front is not flat and thin as assumed in the program and its location as well as width cannot be determined directly from the experimental data. They can,however, be estimated from the VCHP experimental surface temperature measurements. Using those data, the approximate front location as a function of time was established and, after a program modification, could be inputed to HPTRAN rather than calculated from the program equations. With the front then positioned fairly well in the program, a comparison of the computed and experimental panel temperatures provide a reasonable check of the transient operation of the heat pipe system, but primarily for the feeder heat pipes and the panel. Since the actual front location at a given time may itself depend on the transient heat transfer within the VCHP,this approach of inputting to the program the experimental front position does not necessarily provide a check of the computed VCHP transients.

The validation of HPTRAN was the subject of reference 6. Carroll, the author, who also wrote the program, concluded that HPTRAN does simulate transient response of the feasibility VCHP radiator system fairly accurately. In his study, emphasis was placed on the transients associated with starting-up of the VCHP from an "off" condition by increasing the temperature of the coolant entering the system.

Table 3.2 lists the particular time sequences which Carroll used in his program validation. Actually an additional time sequence was included but was omitted in Table 3.2 since the reservoir temperature was not correct.

The present investigator agrees with the conclusion of reference 6, that the program HPTRAN does indeed have merit, and since this was substantially shown in reference 6, the arguments need not be repeated here. Whether the program has been satisfactorily validated is questionable, in the opinion of the present investigator. In that regard it would be worthwhile to take the runs of Table 3.2, for example, and investigate each of them in greater depth than was done in reference 6.

3.3 Results for Time Period 193-07-03 to 193-08-36

To illustrate, consider the time period 193-07-03 to 193-08-36 of Table 3.2, a span of 92 minutes, where T_{IN} was increased from 57^{o}F to 72^{o}F by one large initial rise and later an additional small increase, Fig. 3.1. The reservoir temperature also went up from -39F to -20F, but at a near constant rate, Fig. 3.1. The heat absorbed, Q_A', and the coolant flow rate were nearly constant at 56 Btu/hr-ft^2 and 1870 lb/hr., respectively. This was a sequence 17 run, and in fact, includes the data at time 193-08-30 which were used as a steady-state point of Table 3.1.

DAY-HOUR-MINUTE	$\dot{Q}_A$ BTU/HR-FT^2	T_{IN} °F	$\sim T_R$ °F	FLOW RATE lb/hr	DURATION MIN.
191-16-32	24	58--80	-70	285	64
193-04-18	18	52-66	-56	1924	41
192-10-12	54	63-72	-16	1070	47
193-07-03	56	57-72	-27	1870	92

TABLE 3.2 Time Sequences Used for Program Validation

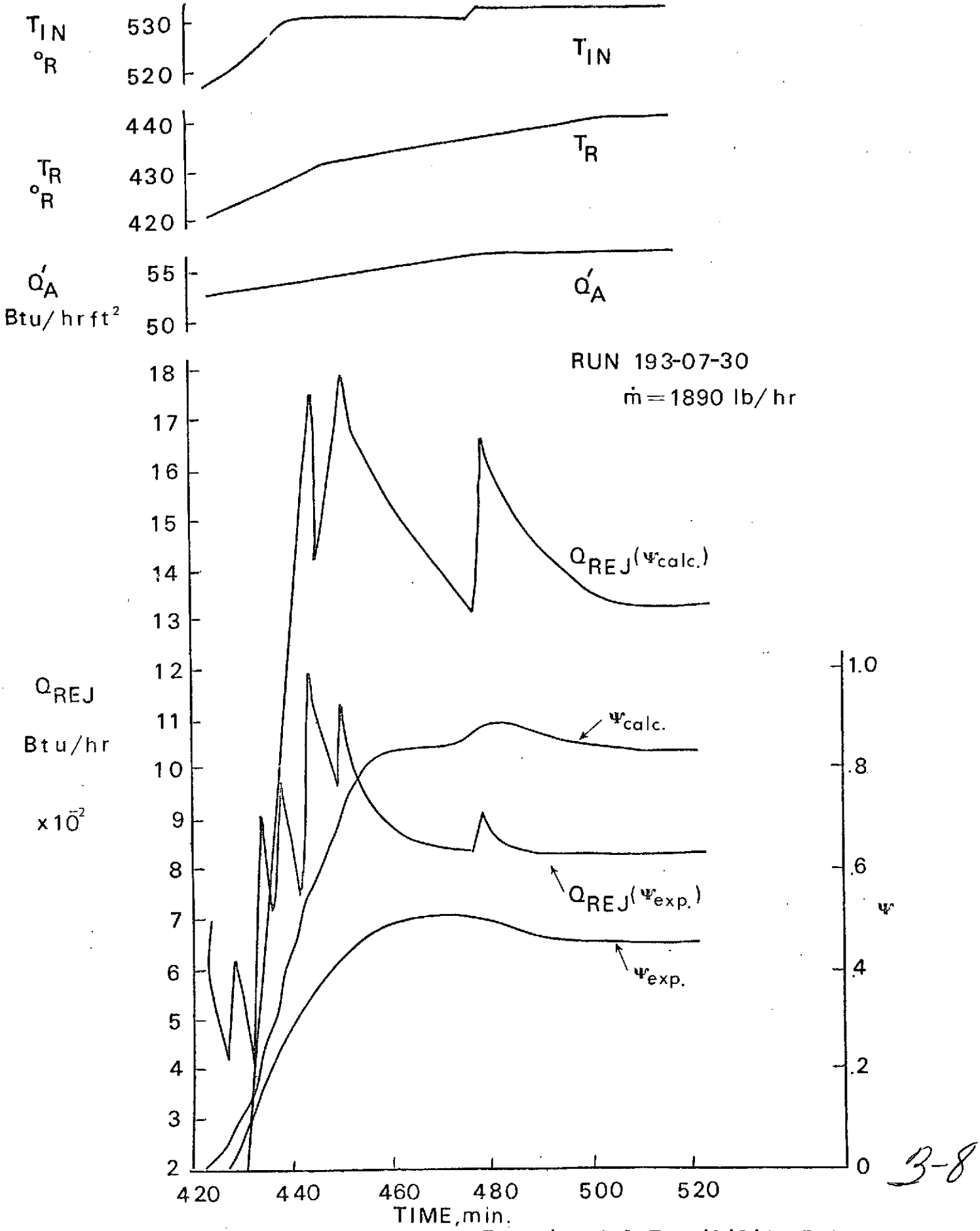

FIGURE 3.1 Calculated and Experimental Feasibility Data for Run No. 193-07-03

The calculated front location expressed by the dimensionless parameter, $\Psi_{calc.}$, and the front location as determined from the VCHP condenser surface temperature measurements, $\Psi_{exp.}$, are also presented in Fig. 3.1. These are the Ψ values used in reference 6 for the time period 193-07-03 to 193-08-36. Referring to the $\Psi_{calc.}$ curve, which is the analytical front location as calculated from HPTRAN, according to reference 6 it is calculated from:

$$\Psi = 1 + \frac{\left[\left(\frac{V_R}{V_c}\right)\frac{(P_V - P_{V_R})}{T_R} - \frac{m_g R_g}{V_c} \right]}{\frac{1}{N_p}\sum_{i}^{N_p}(P_V - P_{V_s}^{i})/T_s^{i}} \qquad 3\text{-}1$$

where

N_p = Number of nodes on the inactive portion of the VCHP

i = Node number on the inactive portion of the VCHP

In the earlier steady-state program PRFORM, (3), $\Psi_{calc.}$ was obtained from a somewhat different equation:

$$\Psi = 1 + \frac{\left[\left(\frac{V_R}{V_c}\right)\frac{(P_V - P_{V_R})}{T_R} - \frac{m_g R_g}{V_c} \right]}{(P_V - P_{V_s})/T_s}$$

where T_s is the average temperature of the inactive portion of the VCHP. As the VCHP opens during the time period under study the $\Psi_{calc.}$ curve, Fig. 3.1, rises to a value of 0.82 due to the increase of the inlet temperature (in spite of the VCHP closing effect of an increasing reservoir temperature), and then both the T_{IN} and $\Psi_{calc.}$ curves have

leveled-off at the 455 minutes mark. Henceforth, the $\Psi_{calc.}$ curve does not appear to be correct on the basis of the T_{IN} and T_R data of Fig. 3.1. For example, from time 440 to 475 T_{IN} is constant, but T_R increases from $-29^{\circ}F$ to $-25^{\circ}F$. On the basis of Eq. (2-1), and presumably Eq. (3-1), Ψ should decrease accordingly after 440 minutes but with some time lag due to heat storage in the transient mode. A significant effect of T_R on Ψ was found in the steady-state study of reference 1 for nearly the same conditions as in the present discussion. See Fig. 3.2. It would appear that in the HPTRAN calculation of $\Psi_{calc.}$ the reservoir temperature effect has been attenuated, since $\Psi_{calc.}$ does not decrease in the 35 minute period but remains constant. It is difficult to explain this result on the basis of the transient operation and further study is needed.

If $Q_{REJ\ rad}$ is the net heat radiated from the panel, then a heat balance for the entire system gives:

$$Q_{IN} = Q_{REJ} = Q_{Stored} + Q_{out} = Q_{Stored} + Q_{REJ\ rad.} \qquad 3\text{-}2$$

or:

$$C_p \dot{m} (T_{IN} - T_{OUT}) = C \sum_{i=1}^{30} (T_{i_\tau} - T_{i_{\tau-\Delta\tau}}) + \sum_{i=16}^{28} Q_{REJ_{rad}} \qquad 3\text{-}3$$

In Eq. (3-2) the numbers are nodal point designations. At steady state the heat storage term is zero. Thus,

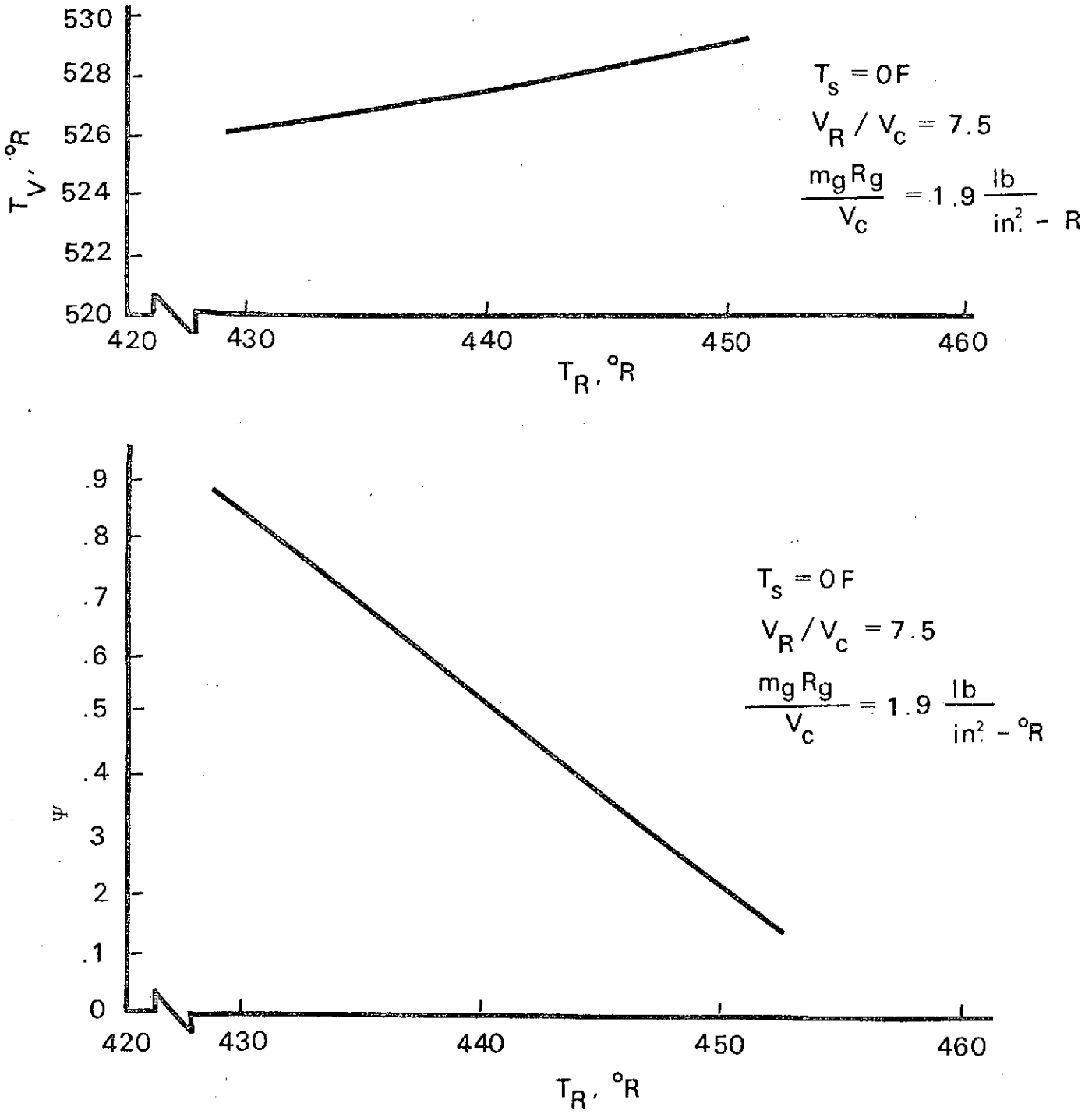

FIGURE 3.2 T_V and Ψ vs. T_R; T_{IN} = 71 F (Run No. 193-08-30)
$\dot{m}$ = 1855 lb/hr, Q'_A = 56 Btu/hr-ft^2

$$C_p \dot{m} (T_{IN} - T_{OUT}) = \sum_{i=16}^{28} Q^i_{REJ_{rad}} = Q_{REJ}$$

In the transient mode Eq. (3-1) may be rewritten:

$$Q_{stored} = C_p \dot{m} (T_{IN} - T_{OUT}) - Q_{REJ_{rad}} = Q_{REJ} - Q_{REJ_{rad}}$$

It can be seen in Fig. 3.1 that Q_{REJ} at time 510 minutes (measured from 193-00-00) calculated by HPTRAN using $\Psi_{exp.}$ has leveled-off at a steady-state value of 813 Btu/hr. The Q_{REJ} value which was calculated from the experimental panel temperatures listed in reference 1, at this time was 980 Btu/hr., and in reasonable agreement with HPTRAN.

Another check of the numerical programs can be made at the 510 minutes point. Referring to Fig. 3.1, the Q_{REJ} value based on $\Psi_{calc.}$ from HPTRAN is about 1320 Btu/hr., and $\Psi_{calc.} = 0.84$. The analytical value given in reference 1 and calculated by the steady-state program PRFORM (3) is 1238 Btu/hr at $\Psi_{calc.} = 0.74$. Ostensibly, the differences between the two programs can be explained by:

a. Some differences in the input data to each of the programs, particularly, T_{IN}, T_R and $m_g R_g / V_c$.

b. Some improvements in the analysis contained in HPTRAN but not PRFORM.

c. The $\Psi_{calc.}$ from HPTRAN being suspect as discussed in the preceding section.

Consider now the transient operation during the start up of the VCHP and referring once again to Fig. 3.1, it can be seen that the Q_{REJ} curves are characterized initially by severe fluctuations and a relative large peak value, 1200 Btu/hr for Q_{REJ} (Ψ_{EXP}). As the VCHP is opened by a rather rapid increase of T_{IN}, one would indeed expect a surge of heat flow into the cold system and a large initial value of Q_{REJ}, but the fluctuations are believed to be due to the numerical method used in the program, and could likely be reduced by increasing the number of nodal points inside the VCHP. This should be considered, as a greater number of nodal points may also significantly improve the accuracy of the results in the transient mode.

Figure 3.3 compares the calculated VCHP and experimental axial wall temperature distribution for three different times, initially (423), 28 minutes later (451), and at the end of the designated time period (516). The calculated values are the Ψ_{EXP} results from HPTRAN. It can be seen that at time 516 minutes the experimental temperatures were lower than the calculated values beyond 28 in. along the VCHP. The experimental data indicate that the VCHP temperatures between 20 inches and 34 inches

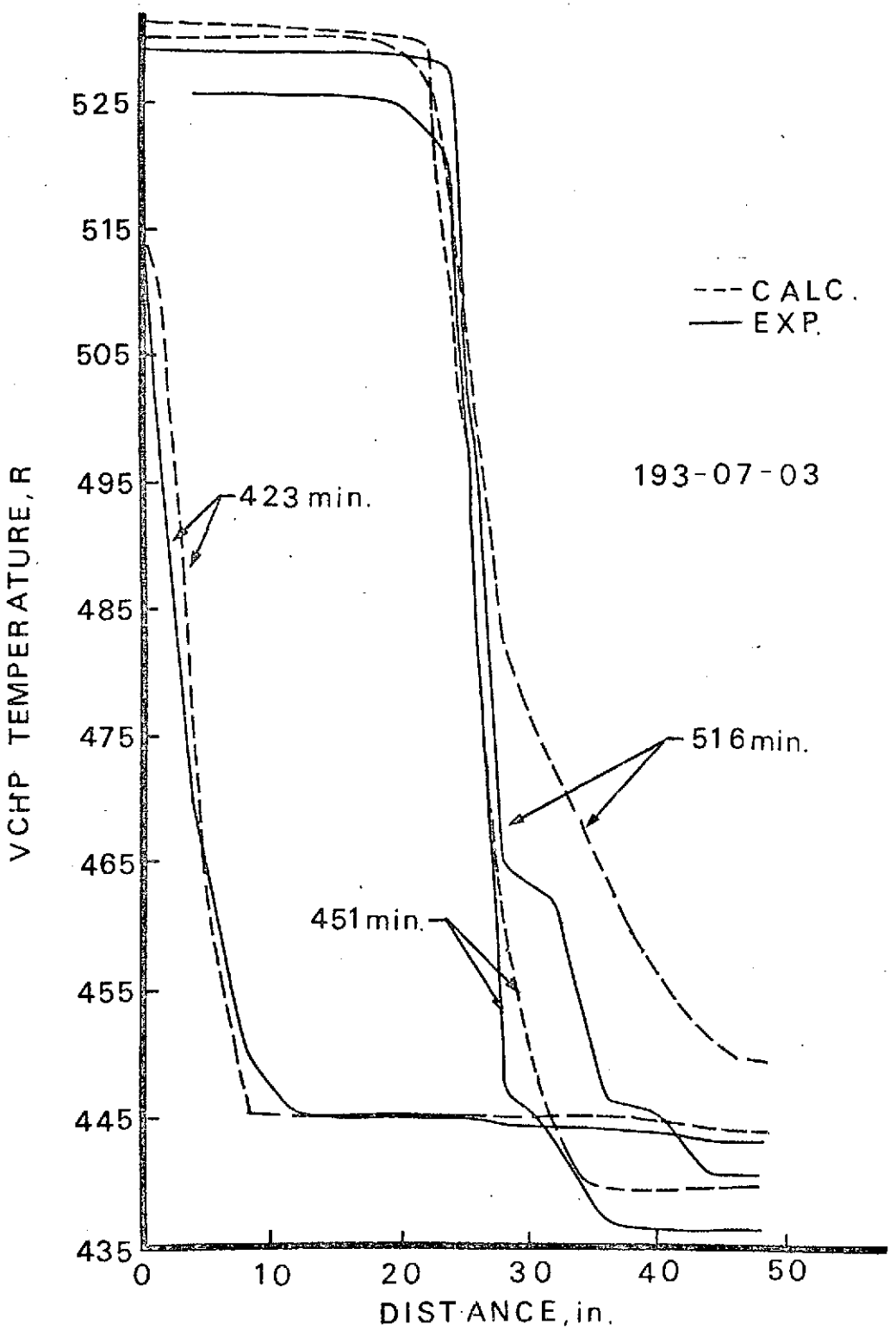

FIGURE 3.3 VCHP Temperature vs. Distance for Run No. 193-07-03

decreased after 464 minutes. This decrease which was not predicted by HPTRAN and may be due to the movement of the front toward the evaporator, heat conduction, or heat leaks, is also brought out in a plot of the VCHP temperatures versus time, Fig. 3.4. The measured decrease of the VCHP temperature at 24 inches (TC 14) is about 15°F in 50 minutes where the HPTRAN results gave only a 3 degree drop!

The panel temperatures versus time are presented in Figs. 3.5 and 3.6. It can be seen that the root temperature of Feeder D, which begins to drop after 480 minutes, is the only measured panel temperature indication of the T_R closing effect which was quite evident in the VCHP data and discussed in detail above. The panel temperature distribution at the end of the time period is shown in Fig. 3.7 where the peak points on the temperature distribution curve are the root temperature of the active and partially active feeders. The "valley" minimum points are located half-way between feeders. Section 4.0 of the report is a study devoted to finding an explanation of why the temperature difference between these two locations, i.e., on the feeder and midway between, is less experimentally than calculated.

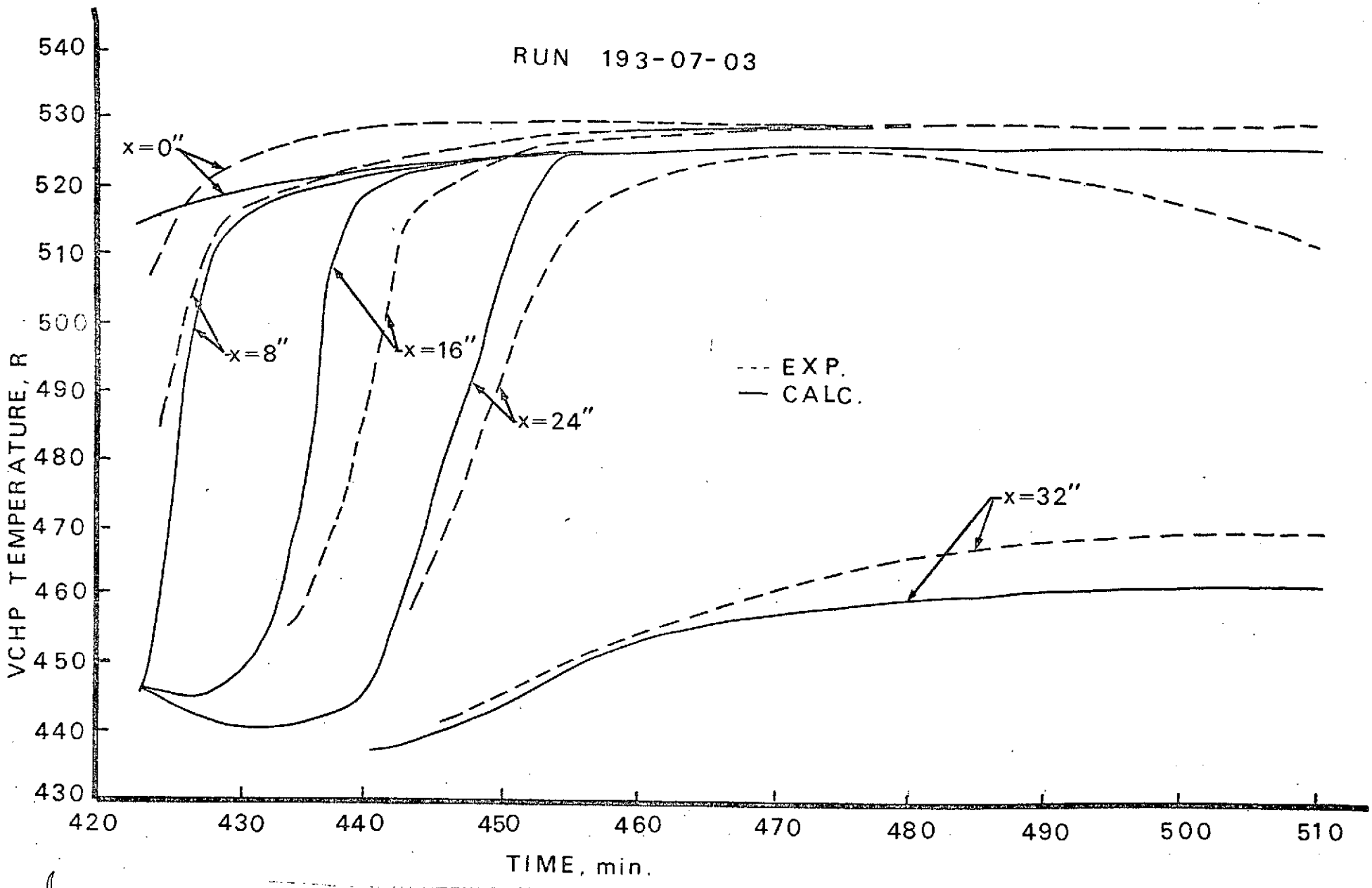

FIGURE 3.4 VCHP Temperature vs. Time for Run No. 193-07-03

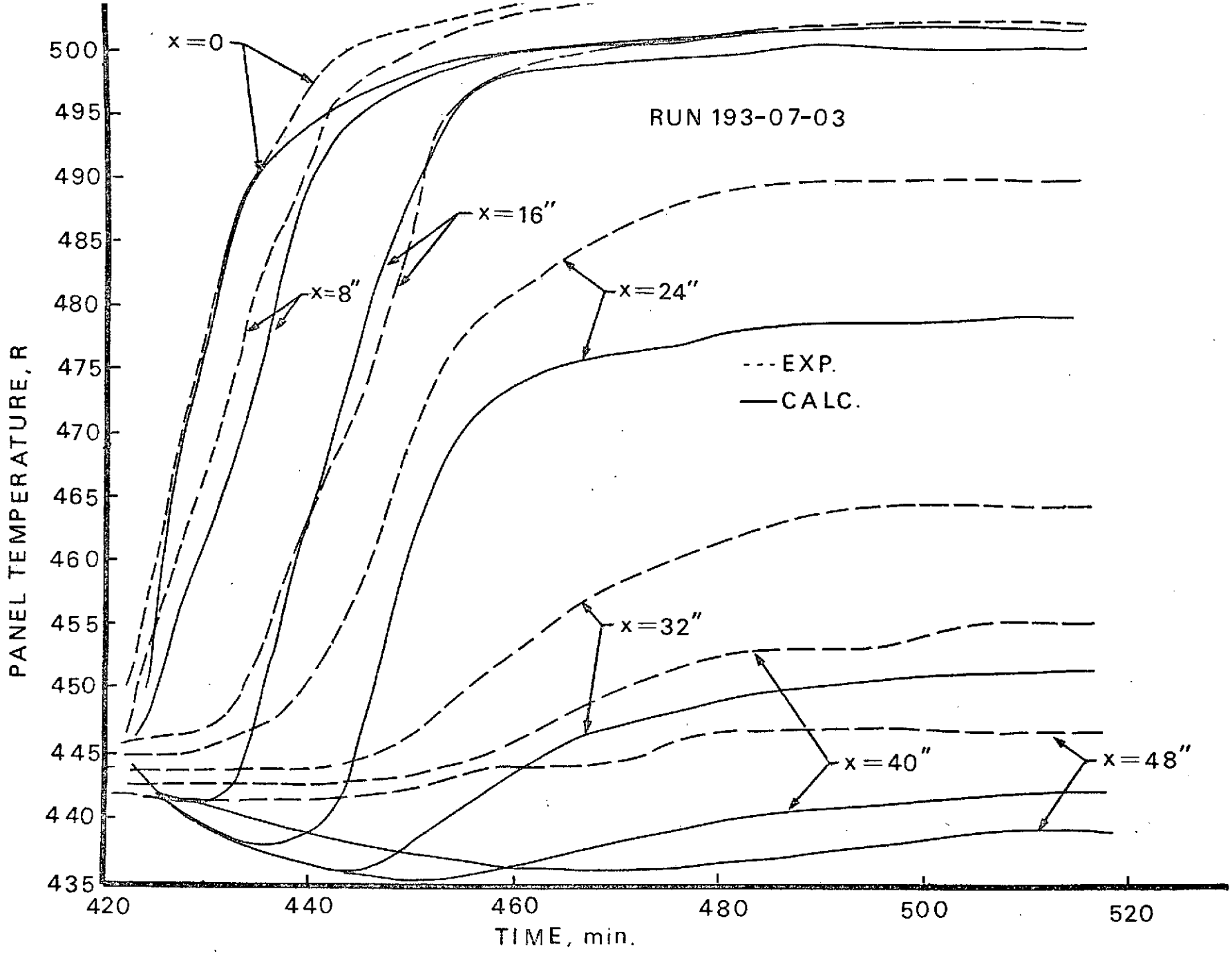

FIGURE 3.5 Panel Temperature vs. Time for Run No. 193-07-03

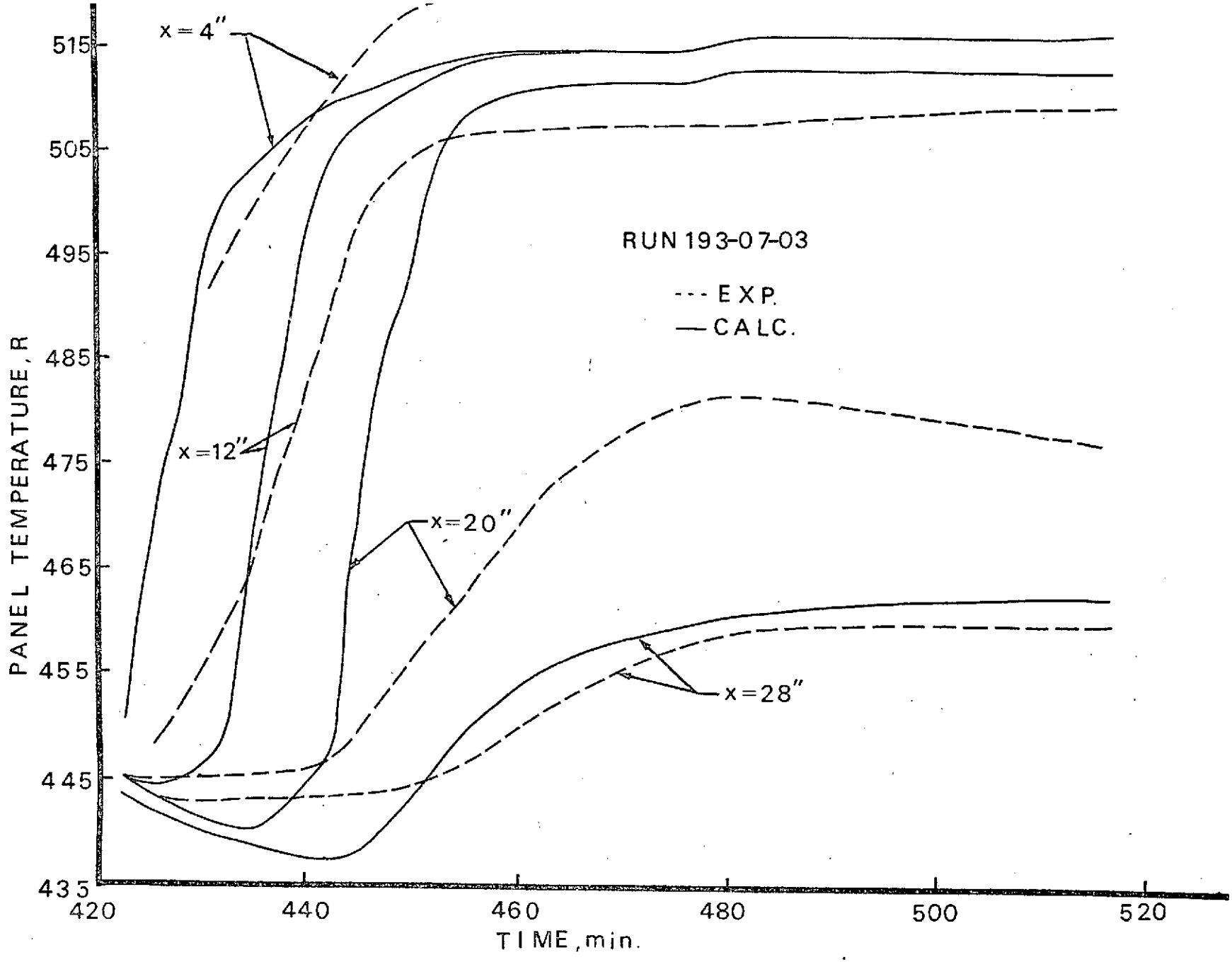

FIGURE 3.6 Feeder Root Temperature vs. Time for Run No. 193-07-03

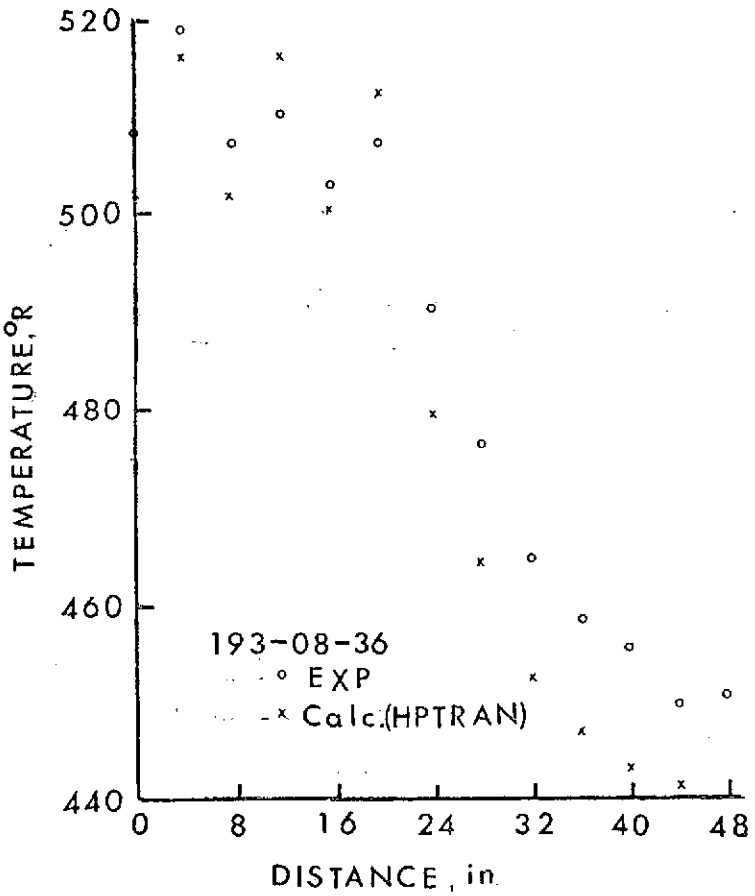

FIGURE 3.7 Panel Edge-to-Edge Temperature Distribution; Time 193-08-36

4.0 PANEL TEMPERATURE DISTRIBUTION

Comparisons made in references 1 and 2 and Section 3.3 of this report between the experimental results obtained from the feasibility tests and the computer data have brought out that a consistent disagreement exists in the temperature distribution on the panel fin between active feeders. That is, considering two adjacent active feeders, the difference between the two high panel temperatures, located on the feeder heat pipes, and the minimum temperature at the mid-point position between feeders, was consistently less than the calculated temperature difference for corresponding points on the panel.

The comparisons are presented for the runs of Table 3.1 in Figs. 4.1 - 4.6 and Table 4.1, where the computer data were obtained from the steady-state program PRFORM. Referring to Table 4.1, it can be seen that the theoretical temperature difference $T_{nR_{FHP}} - T_p = \Delta T_p$ is several degrees greater than experimental. For example, by 3 to 6 degrees for feeder A, by 6 to 13 degrees for feeder B, and by 5 to 9 degrees for feeder C. The magnitude of ΔT_p depends upon the quantity of heat Q being conducted away from the feeder heat pipe through the panel. Thus, to insure that $Q_{exp} \geq Q_{calc.}$ consider run 193-15-18 where $Q_{REJ\ exp} > Q_{REJ\ calc.}$ by

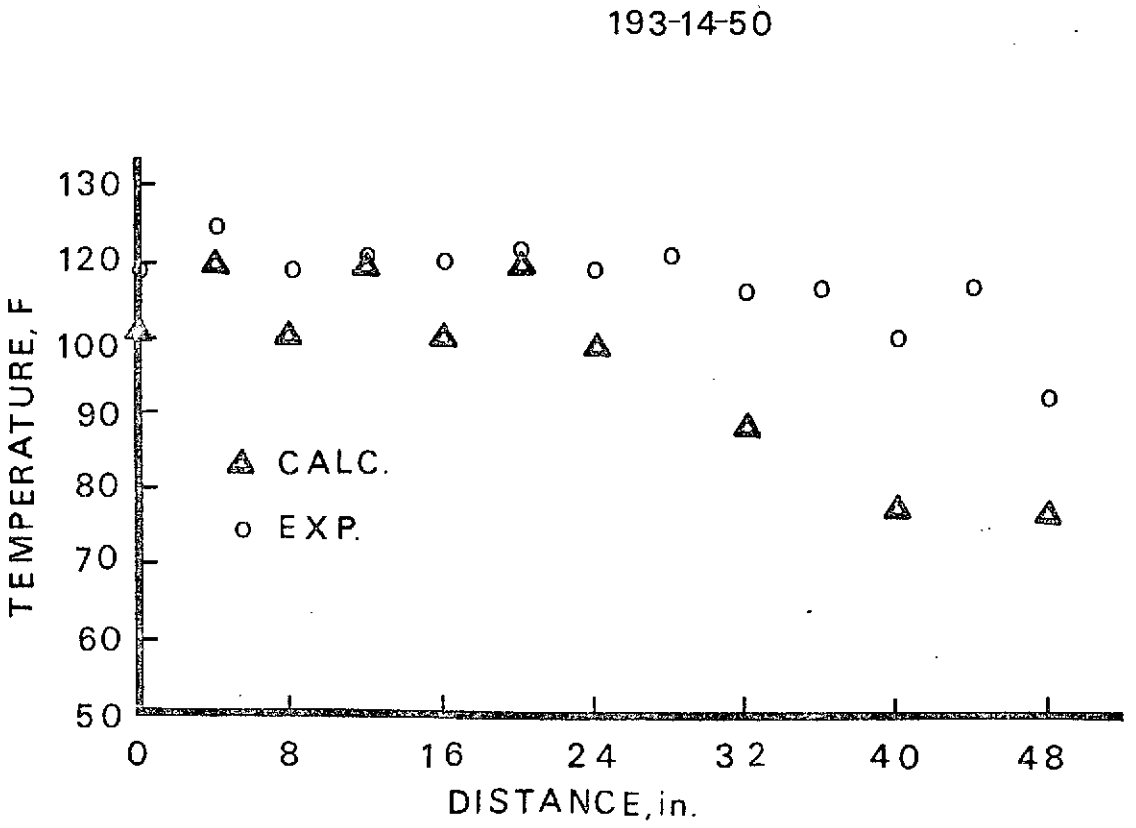

FIGURE 4.1 Panel Edge-to-Edge Temperature Distribution; Time 193-14-50

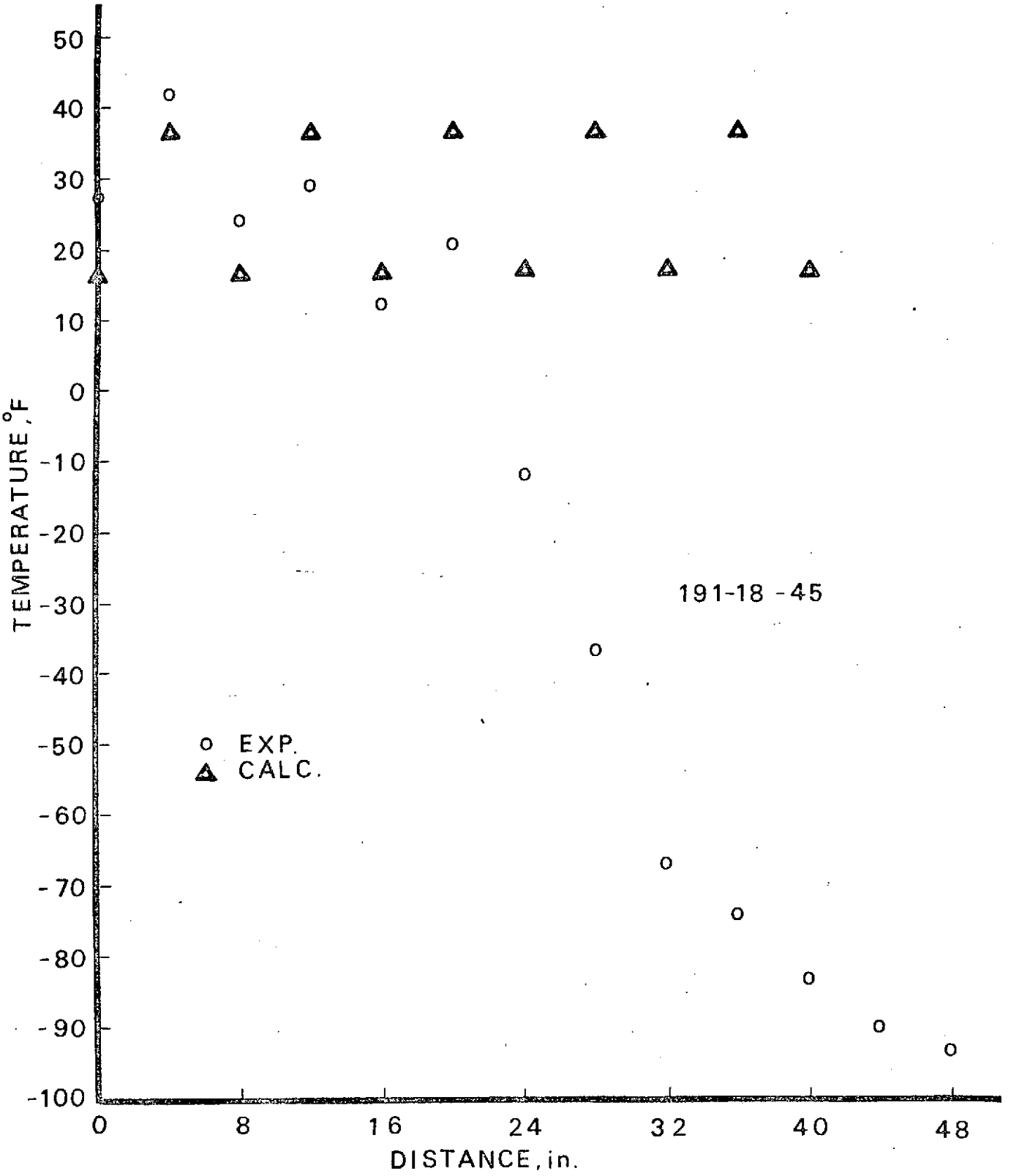

FIGURE 4.2 Panel Edge-to-Edge Temperature Distribution; Time 191-18-45

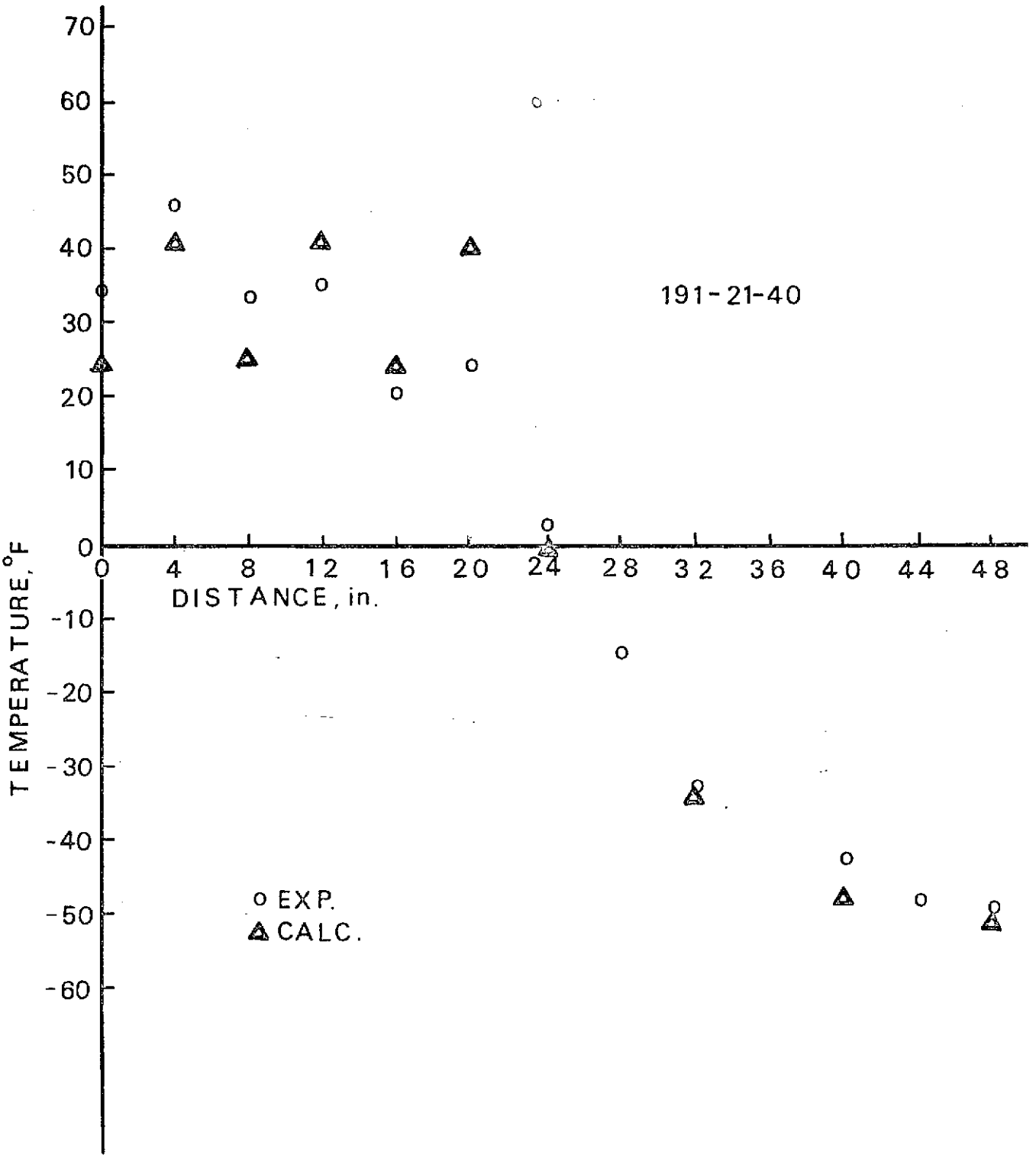

FIGURE 4.3 Panel Edge-to-Edge Temperature Distribution; Time 191-21-40

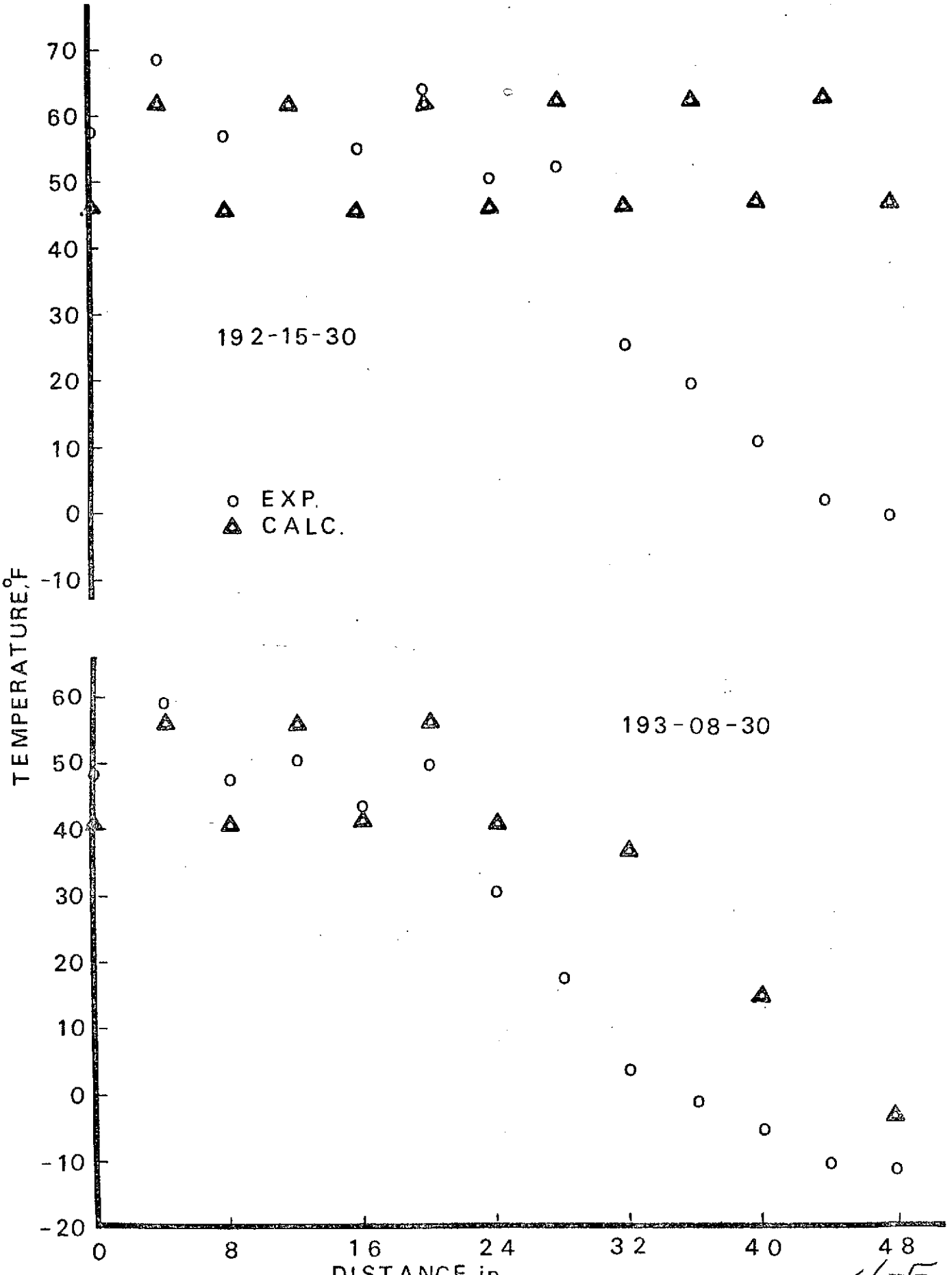

FIGURE 4.4 Panel Edge-to-Edge Temperature Distribution; Times 192-15-30 and 193-08-30

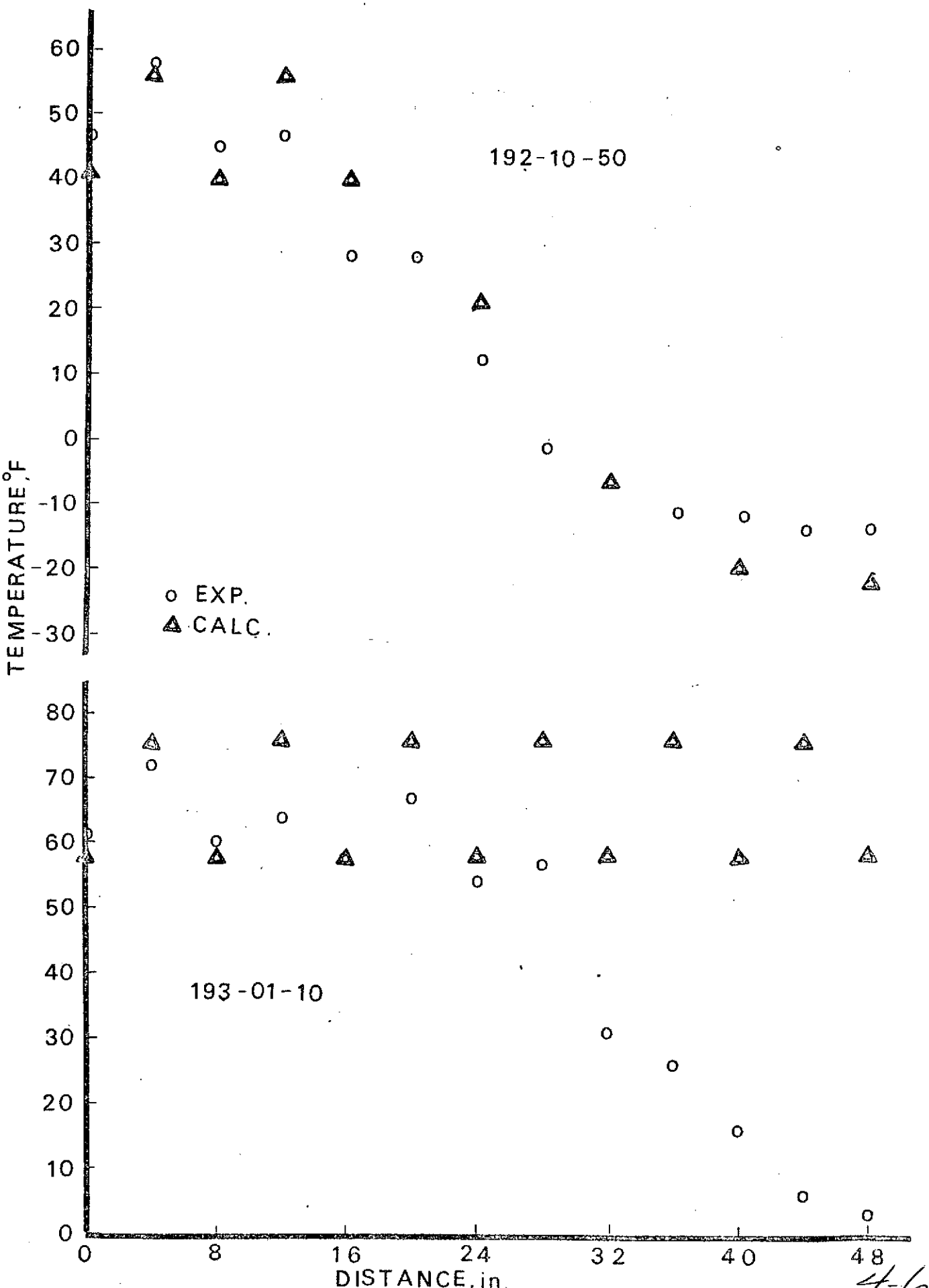

FIGURE 4.5 Panel Edge-to-Edge Temperature Distribution; Times 192-10-50 and 193-01-10

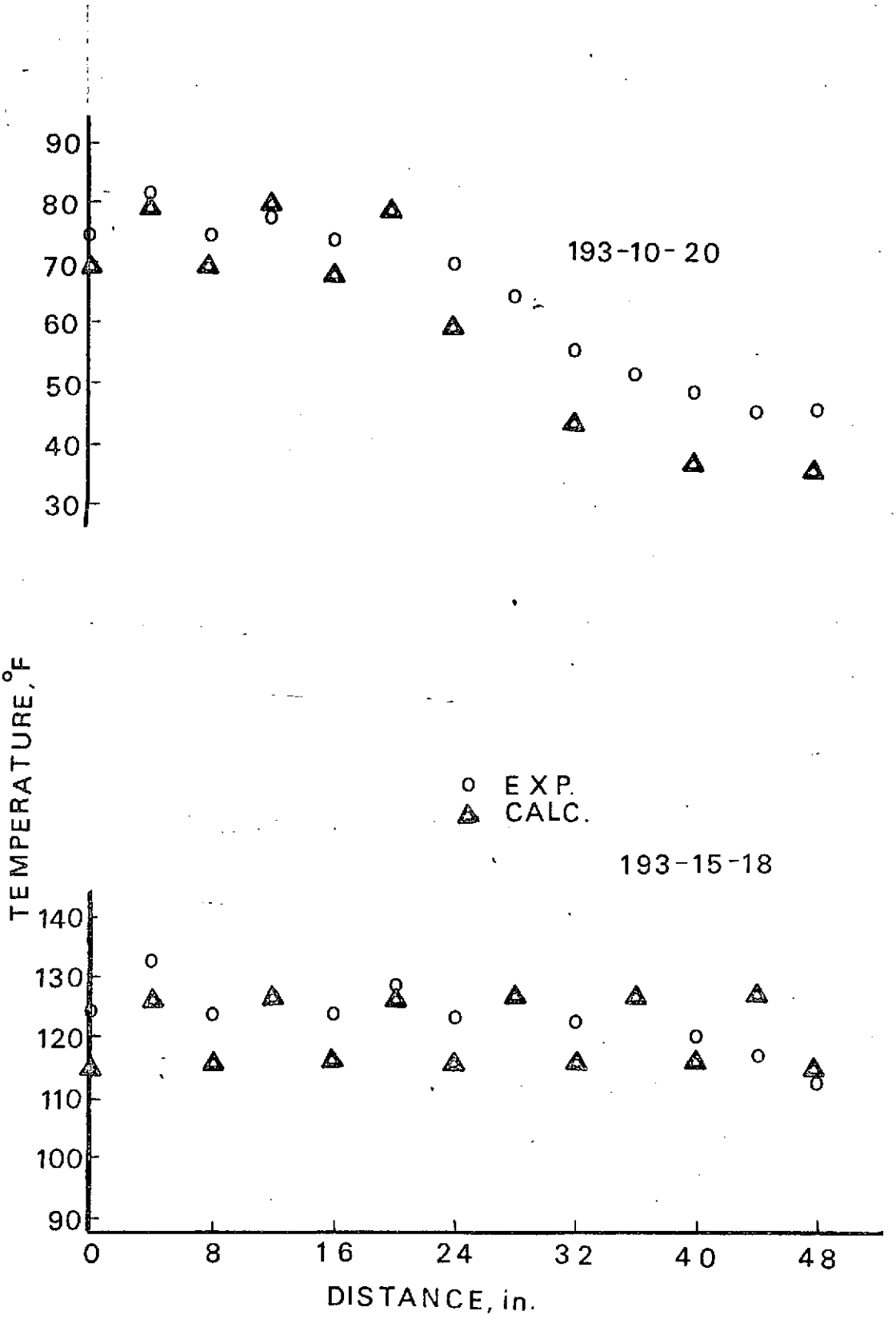

FIGURE 4.6 Panel Edge-to-Edge Temperature Distribution; Times 193-10-20 and 193-15-18

	ΔT_p, °F				$\Delta T_{p_{calc}} - \Delta T_{p_{EXP.}}$, °F		
RUN NO	FEEDER A	FEEDER B	FEEDER C	CALC.	FEEDER A	FEEDER B	FEEDER C
191-18-05	17	NA	NA	21	4	--	--
191-18-45	16	NA	NA	20	4	--	--
191-21-40	12	NA	NA	16	4	--	--
191-15-30	12	5	9	16	4	11	7
192-10-50	11	NA	NA	16	5	--	--
193-08-30	11	NA	NA	15	4	--	--
193-01-10	12	5	9	18	6	13	9
193-10-20	7	4	5	10	3	6	5
193-14-50	6	1	2	10	4	9	8
193-15-18	9	3	5	12	3	9	7

NA = Feeder not fully active.

TABLE 4.1 Panel Fin-Length ΔT_p.

20 percent (see Table 3.1). From Table 4.1 for run 193-15-18, $\Delta T_{p\ FHP_{calc}} > \Delta T_{p\ FHP_{exp}}$ by 3^{o} for feeder A, by 9^{o} for feeder B and by 7^{o} for feeder C. It can be concluded, therefore, that the measured panel ΔT_{p} between the feeder and the midpoint between feeders was significantly less than predicted by the analysis.

The radiation from a point on the panel varies with the fourth power of the local temperature so a few degrees of panel temperature inaccuracy can have a large effect on Q_{REJ}. Since the panel temperature distribution is crucial to the proposed optimization study of the panels, an effort was made under the present contract to understand these experimental results and to make any corrections to the analysis found necessary.

The afore-mentioned discrepancy between the analytical and experimental results was surprising, since the problem is unrelated to the efficiency of operation of heat pipes and would appear to be simple heat conduction in the panel with radiation to and from the panel surface facing the simulator. The opposing surface of the panel was insulated in the tests and is considered an adiabatic in the computer program PRFORM.

PRFORM results are obtained from a model consisting of a nodal point located on each of the feeders plus three

nodal points equally spaced between feeders. One-dimensional heat transfer perpendicular to the feeders was assumed. For convenience, in the present study of the panel temperature distribution a separate small computer program was written to exepedite a parametric study of an isolated section of the panel located between two active feeders. In this small program, titled SNOD, originally the number of nodal points between feeders was set at seven, four more than in PRFORM. In addition, results obtained from a computer program FIN 1 (7) (9 nodal points) were compared with the experimental data.

4.1 Effect of Heat Transport in Feeder, Q

Figure 4.7 shows that ΔT_p increases linearly with Q. Since Q for an individual feeder cannot be measured experimentally, it is difficult to compare analytical and experimental results for the same Q value. For this reason, it is desirable that $Q_{EXP} > Q_{calc.}$ to conclude that $\Delta T_{p\ exp} < \Delta T_{p\ calc.}$. This was illustrated above for run 193-15-18.

4.2 Comparison of Results from Different Programs

The panel temperature distribution calculated from three computer programs, PRFORM, SNOD and FIN each using different numerical methods are compared in Fig. 4.8. The conditions chosen correspond to run time 193-10-20. It is seen that good agreement exists between the results from

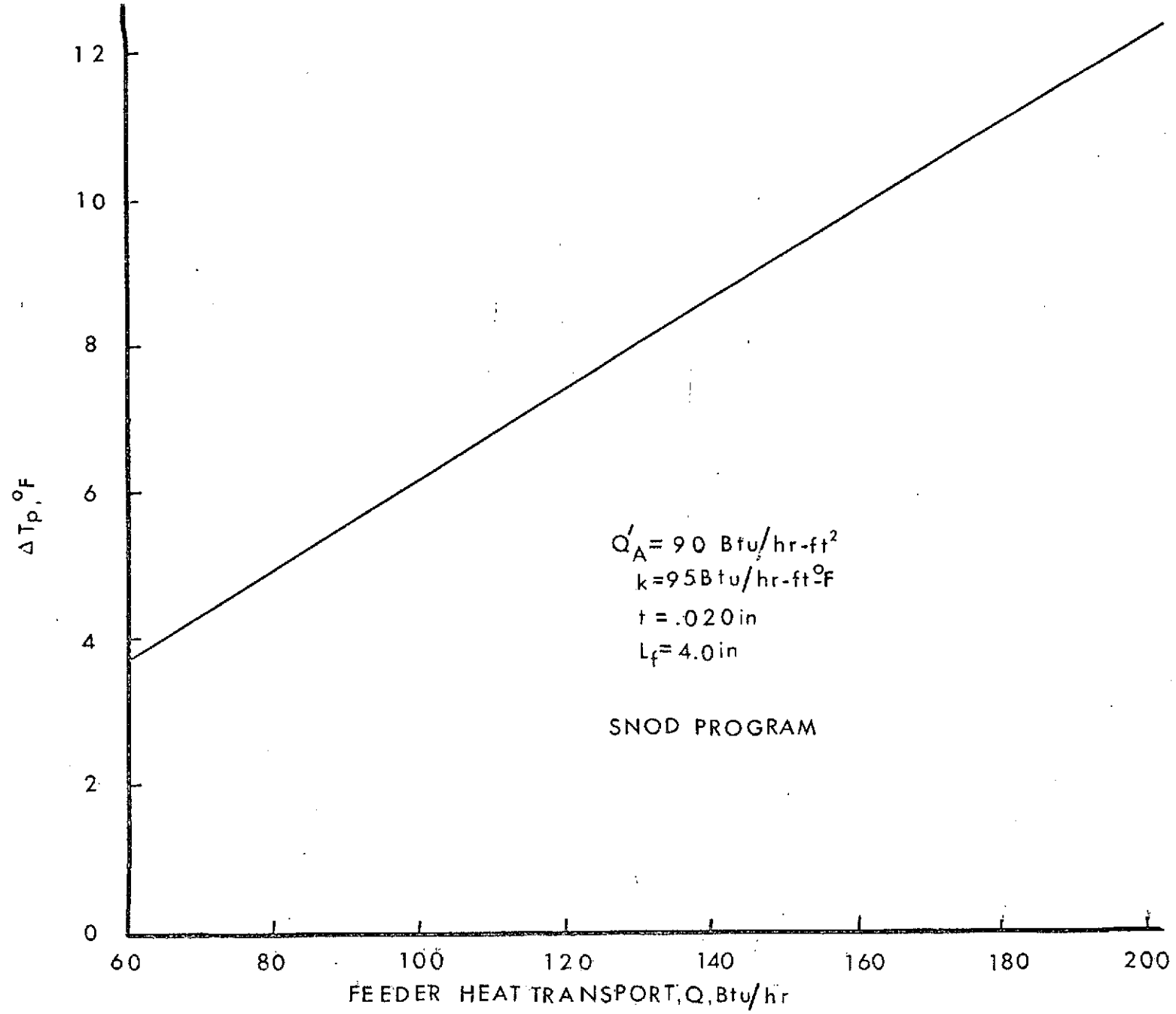

FIGURE 4.7 Effect of Fin-Heat Transfer on Fin-Length ΔT_p

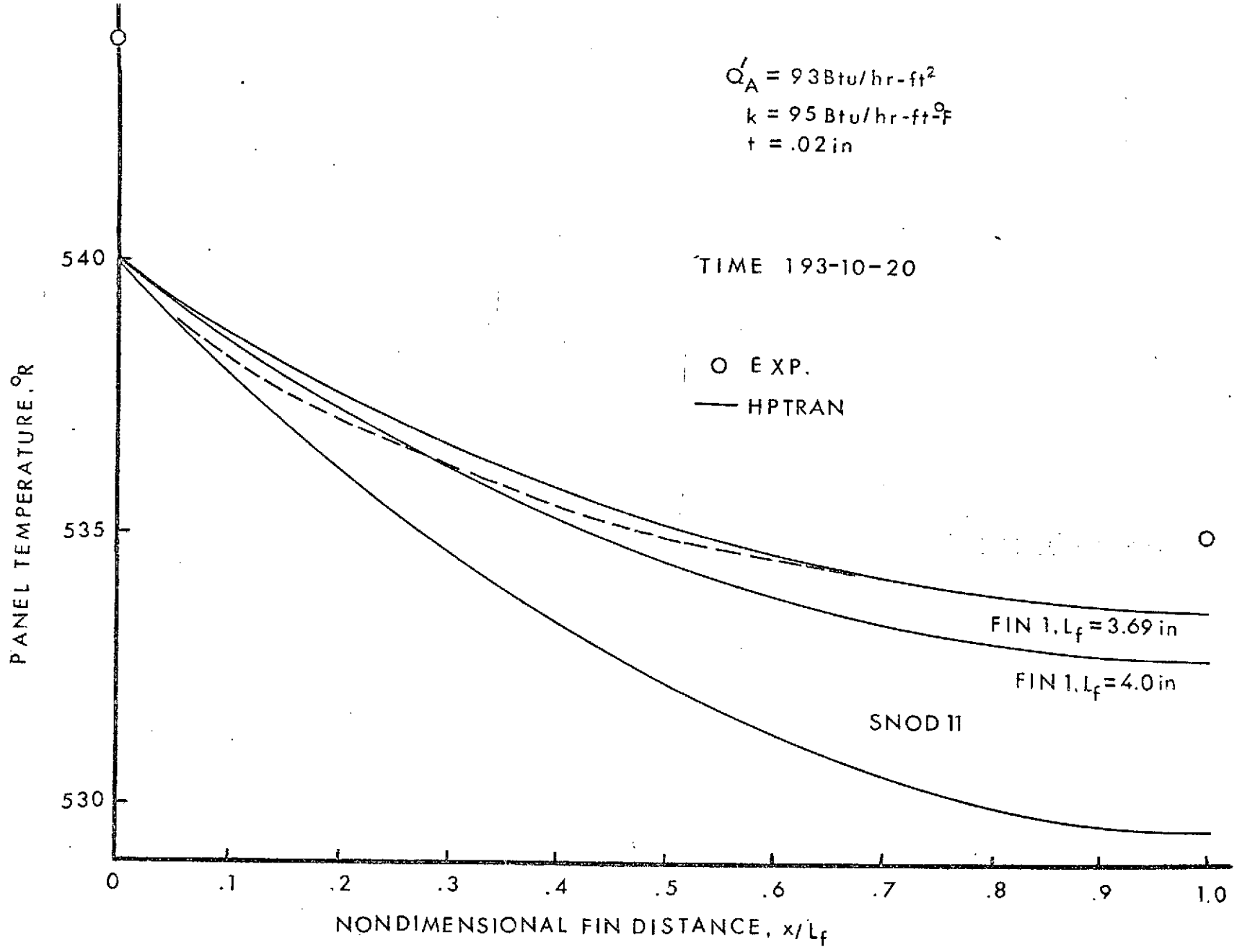

FIGURE 4.8 Comparison of Panel Temperatures Calculated from Different Computer Programs

PRFORM and SNOD, but FIN produced a flatter temperature profile which gives $\Delta T_{p\ calc.}$ in closer agreement with the experimental results, but before any conclusions can be drawn Q must also be compared. The feeder heat-transport Q is input in SNOD but is calculated from the output from the other two programs:

$$Q = C_{2n} (T_V - T_{nR}) \text{ PRFORM}$$

$$Q = -kA \left(\frac{dT}{dx} \right)_{x = 0} \text{ FIN}$$

Q calculated from the FIN temperature curve, Fig. 4.8 is unrealistically low, 112 Btu/hr compared to 170 Btu/hr for the other two programs. It would appear, therefore, that the actual temperature distribution is approximately as depicted by the sketched-in dashed curve of Fig. 4.8. Unfortunately, an insufficient number of temperature measurements were taken to draw the actual temperature distribution.

4.3 Effect of Panel Thermal Conductance on $\Delta T_{p\ calc}$.

An increase of the panel thermal conductivity from 85 to 100 Btu/hr-ft-F (18 percent) reduced $\Delta T_{p\ calc.}$ from 8 to 7°F or 1°, Fig. 4.9. The nominal value of k is 95 Btu/hr-ft-F. It is reasonable to assume that the true value of k is within 18% of this nominal value. Thus, it is concluded that an incorrect value of k in the programs cannot explain their disagreement with the experimental results.

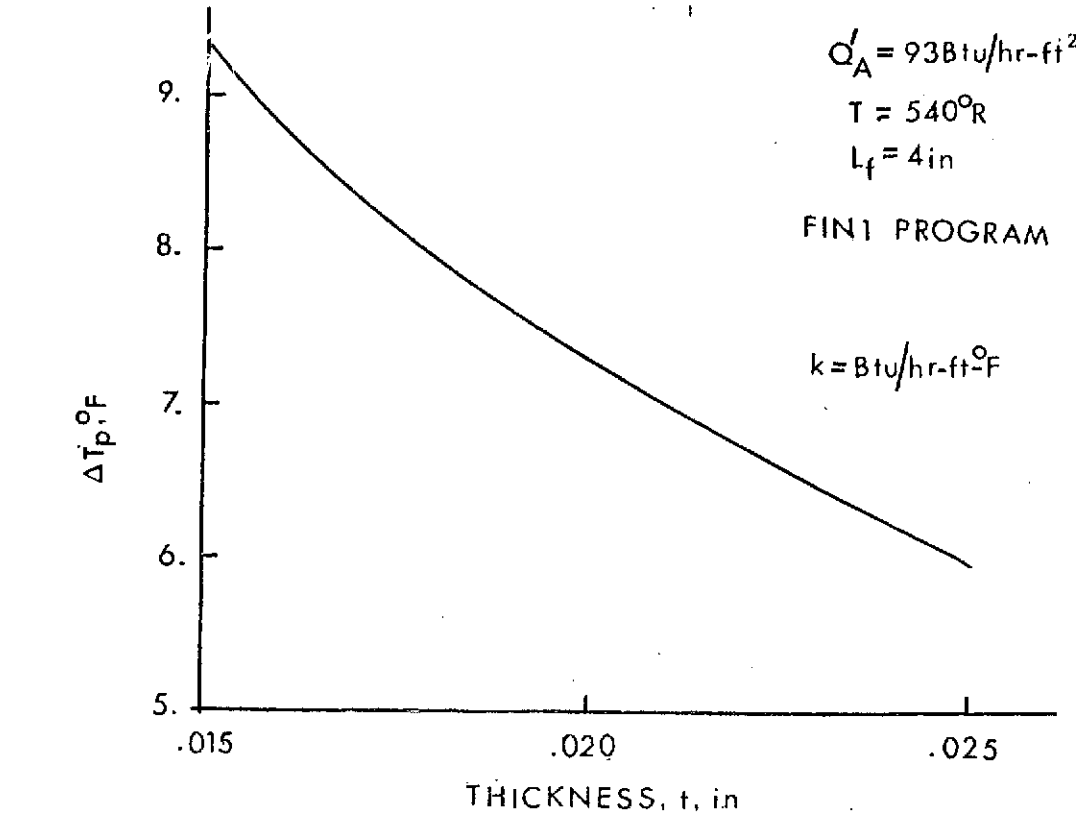

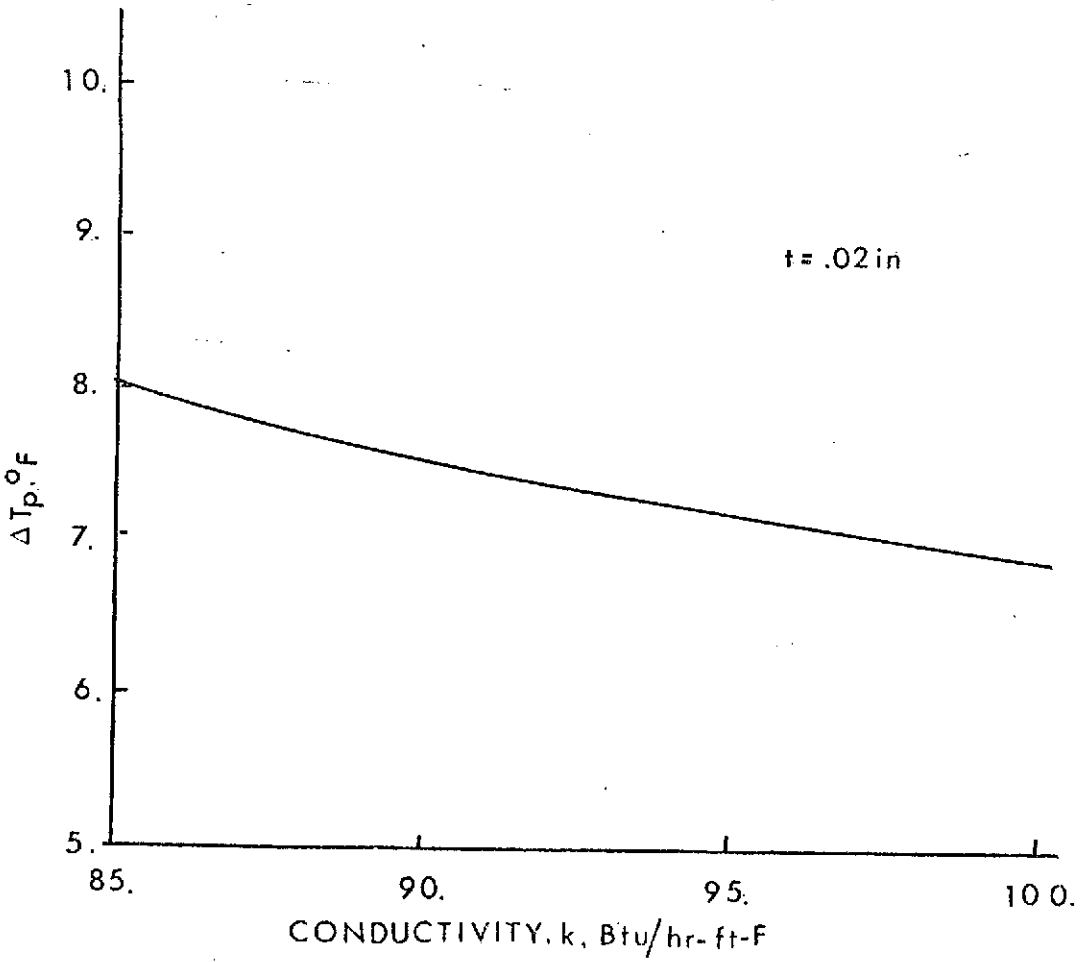

FIGURE 4.9 Effect of Panel Thickness and Thermal Conductivity Fin - Length ΔT_p

An increase of the panel thickness from 0.0185" to 0.0215" (16 percent) reduced $\Delta T_{p\ calc.}$ from 7.8 to 6.9°F or about 1°F, Fig. 4.9. A nominal value of 0.020" is used in the calculations.

4.4 Effect of Q_A' on $\Delta T_{p\ calc.}$

An increase of Q_A' with Q constant increases the magnitude of the panel temperatures but has little effect on $\Delta T_{p\ calc.}$, Fig. 4.10. In the normal program calculation it is assumed that Q_A' is uniform across the panel. An investigation was made to determine the effect on $\Delta T_{p\ calc.}$ of a higher Q_A' value midway between feeders than at the feeders. For simplicity, a straight line variation of Q_A' was assumed. The results are shown in Fig. 4.10. For example, a variation of Q_A' from 82.5 to 92.5 Btu/hr-ft^2 gave little reduction in $\Delta T_{p\ calc.}$ compared to when Q_A' was constant at 93 or 80 Btu/hr-ft^2.

4.5 Effect of Panel Insulation

The panel simulator was wrapped in insulation after its installation in the large vacuum chamber. A simplified analytical attempt was made to determine if the insulation could explain the observed temperature distribution.

Referring to Fig. 4.11,

$$Q = q_{\text{simulator}} + q_{\text{insulation}}$$

$$= A\, h_{rs}\, (T_n - T_E) + A h_{ri}\, (T_n - C T_E)$$

- where $C = Ti/T_E$

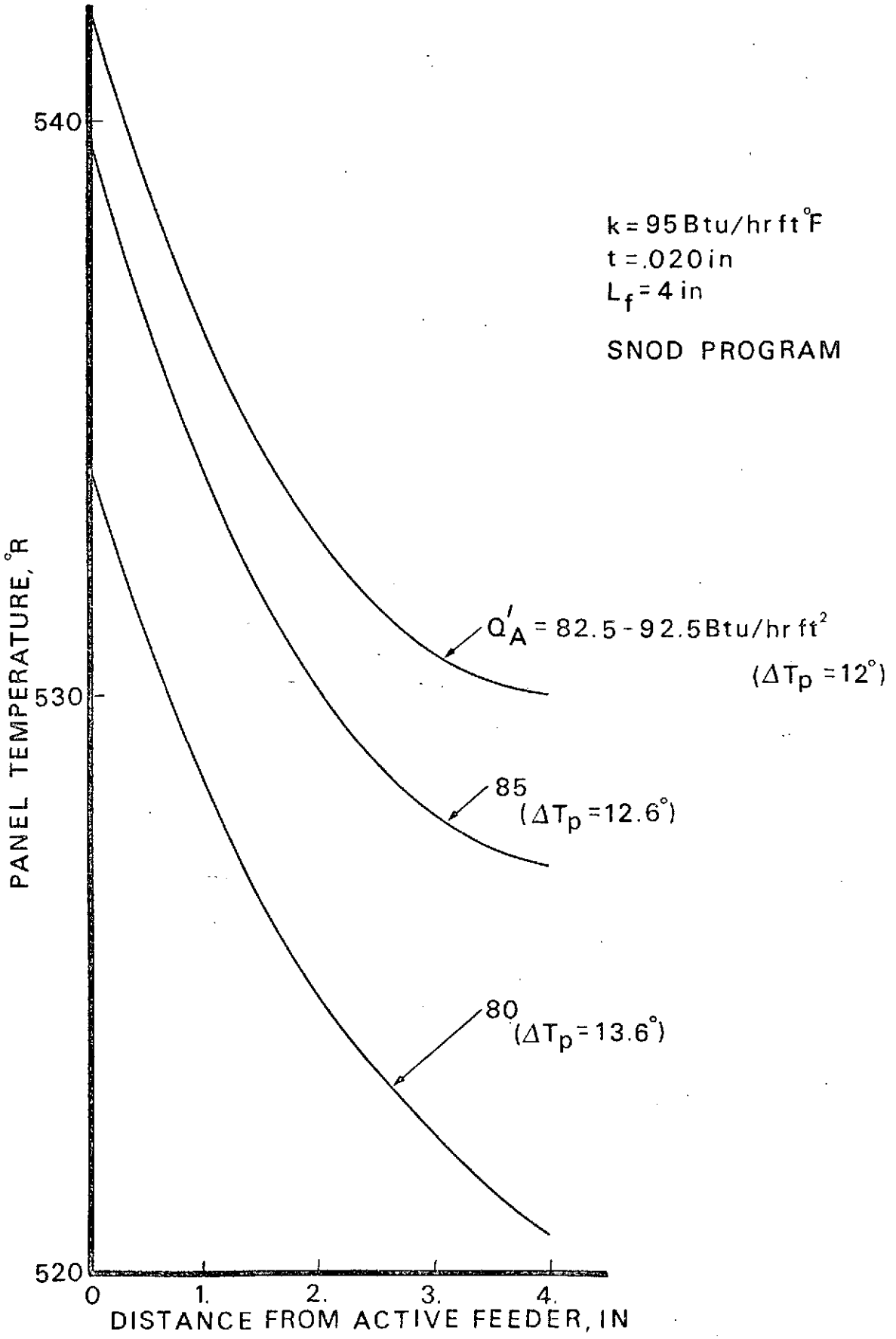

FIGURE 4.10 Effect of Absorbed Heat Flux Q'_A on Panel Temperatures

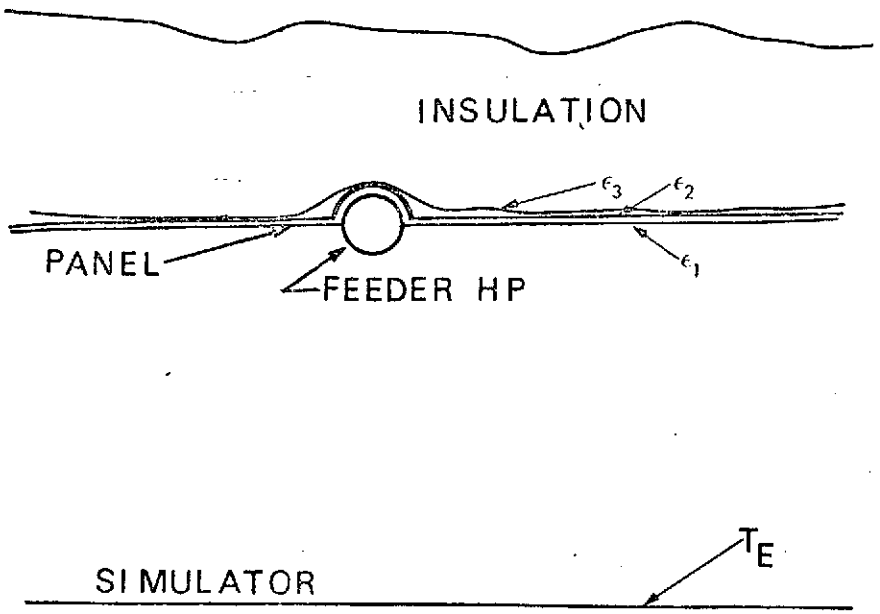

FIGURE 4.11 Panel-Insulation-Simulator Model

At low environment temperatures, in most runs, it is expected that the insulation temperature exceeded the environment temperature, hence $C > 1.0$, perhaps 1.0 - 2.0. At high environment temperatures, $T_i \approx T_E$ and $C \approx 1.0$.

It can be seen from Fig. 4.12 that $\Delta T_{p\ calc.}$ decreases as C increases. Unfortunately, the flat temperature distribution observed in the tests occurred at high environments as well as low environments. Thus, the insulation does not appear to be the explanation for the observed panel temperature profile.

4.6 Effect of Fin Length

If the radius of the feeder heat pipes is considered, the distance from the feeder outside wall to the midpoint between feeders, or fin length, is reduced from 4" to 3.69", Fig. 4.13. The shorter fin length when used in the FIN program reduced ΔT_p by about 12%. Thus, some of the discrepancy can be eliminated by considering the true feeder envelope rather than an imaginary line heat source as is presently assumed in the computer models.

4.7 Effect of Panel $\frac{\alpha}{\epsilon}$ Ratio

Using the FIN program α/ϵ was varied from 0 to 1.1 ($\epsilon = 0.9$), and the results are presented in Fig. 4.14. It can be seen that $\Delta T_{p\ calc.}$ decreases as α/ϵ increases. Normally this ratio is taken as unity. It is unlikely that

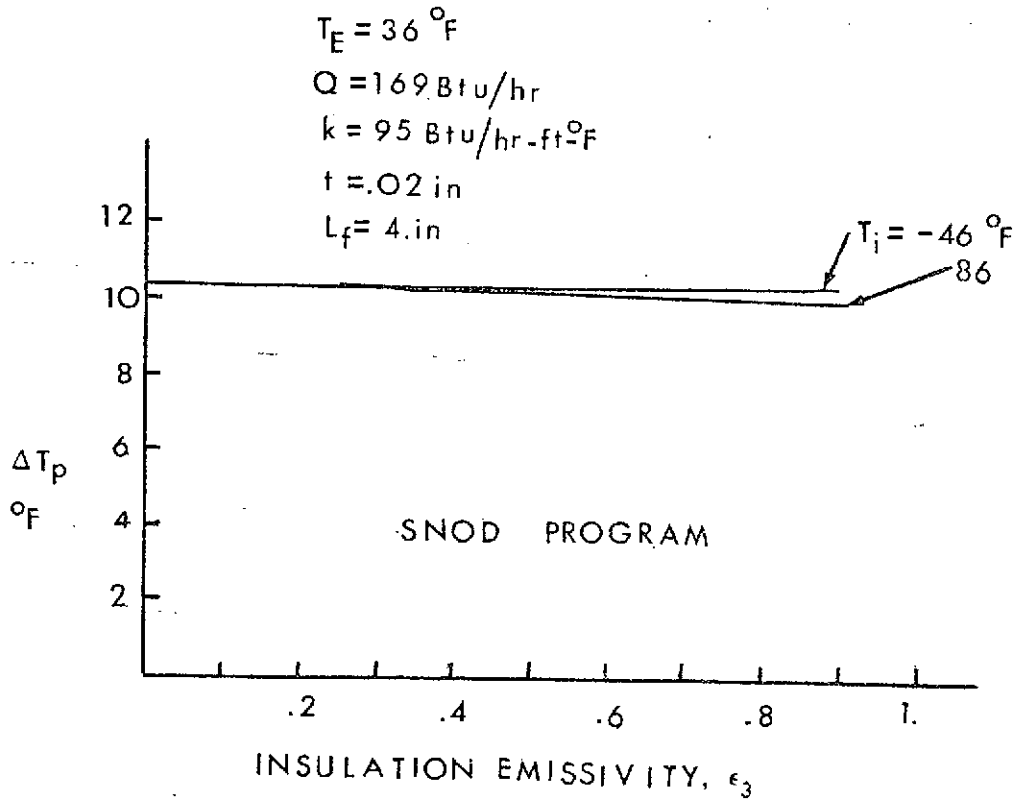

FIGURE 4.12 Effect of Insulation Emissivity and Temperature on Fin - Length ΔT_p

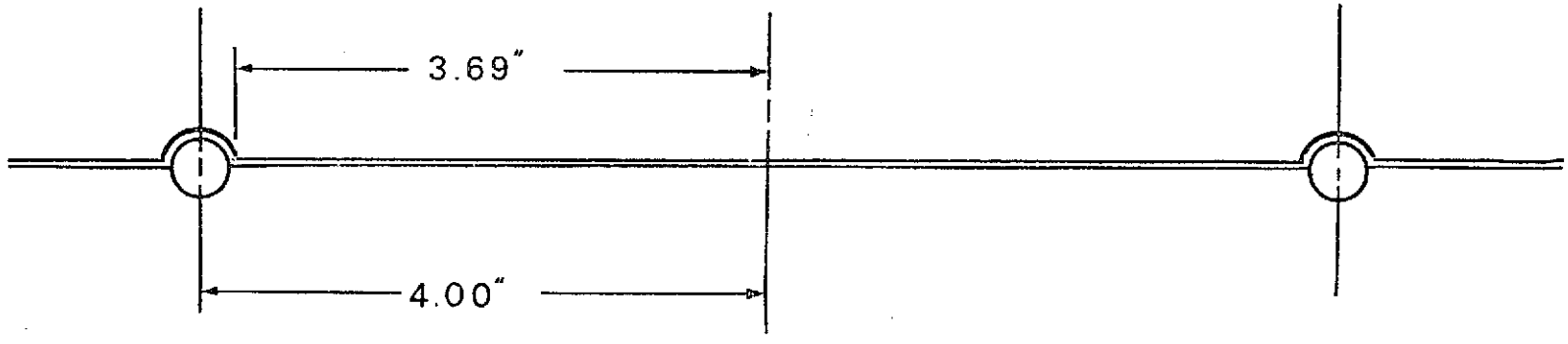

FIGURE 4.13 Feeder Pipes and Fin

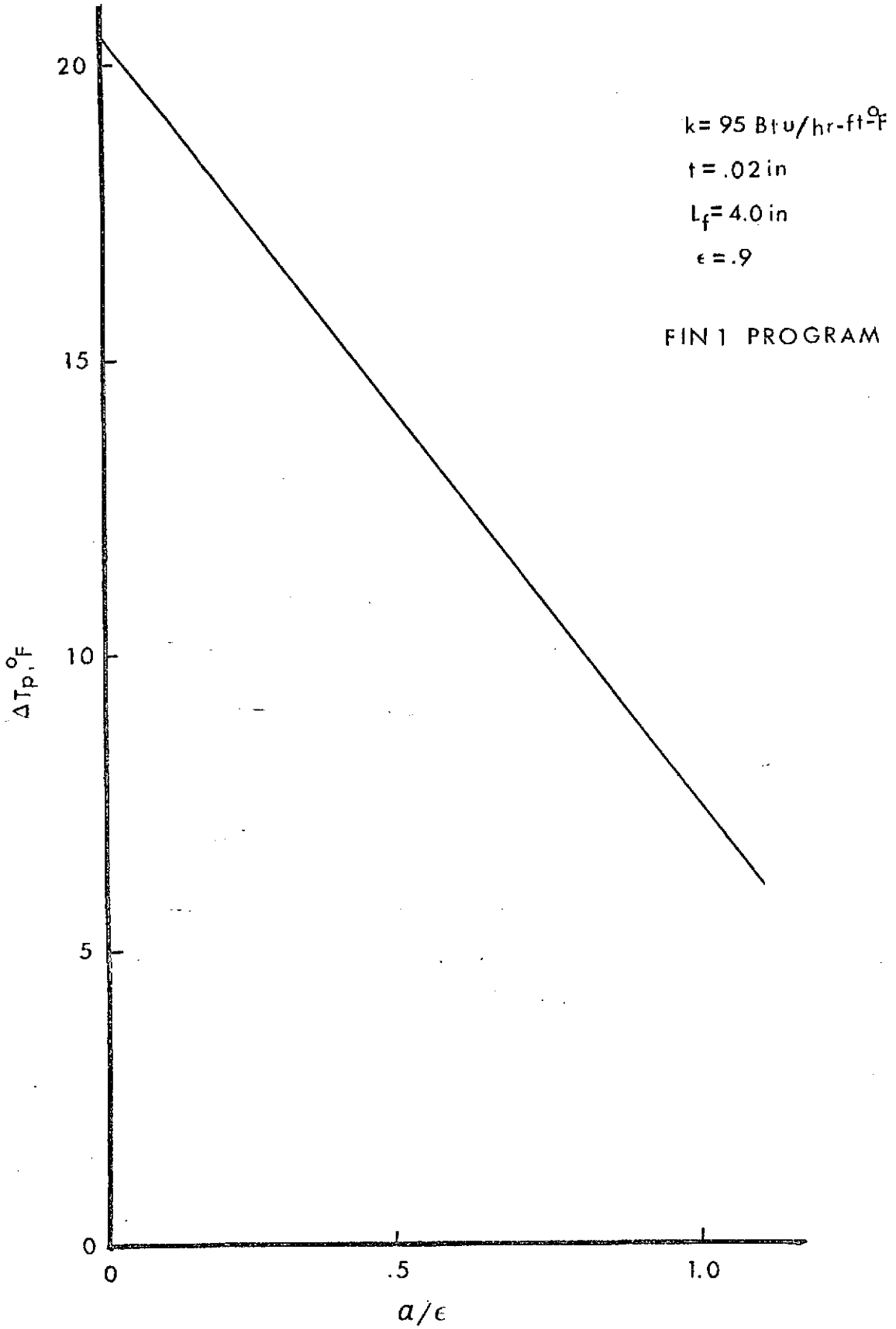

FIGURE 4.14 Effect of Panel a/ϵ Ratio on Panel Fin - Length ΔT_p

α/ϵ was greater than unity in the feasibility tests. Thus, the experimental panel temperature distribution cannot be explained by $\epsilon \neq \alpha$.

4.8 Effect of Number of Nodal Points

The number of nodal points between the feeder and the midpoint between feeders was increased from three to nine. It is seen Table 4.2, that the increase had negligible effect on ΔT_p calc.

Number of Nodal Points	Distance from Active Feeder, in.		
	0	2	4
Five	540R	532.1R	529.6R
Eleven	540R	532.2R	529.6R

TABLE 4.2 Comparison of Panel Temperatures for Five and Eleven Node Models

5.0 CONCLUSIONS

a. With an environment of -83° to -90°F, the feasibility VCHP began to malfunction before it was 1/4 open.

b. With an environment of -13° to -20°F, the data indicate that the feasibility VCHP was operating satisfactorily up to inlet temperatures of 70°F or until the VCHP was about .4 open.

c. The feasibility VCHP watt-in. transport capacity improved at the higher environments and operating temperatures. At the highest environment temperature, 105°F, which was off-design, the VCHP performance exceeded the analytical value.

d. The inlet temperature measurement, AJ 0020, is suspect, particularly for transient conditions.

e. An estimate of the maximum vapor-gas front movement in the direction of increasing the active portion of the VCHP condenser as a result of a severe thermal shock was from 0 to 3/5 fully-open in about 4 min. The indications were that the thermal response of a correctly functioning VCHP would be relatively fast as expected.

f. Chronologically, the VCHP was malfunctioning from the outset of the test program.

g. The VCHP was Q_{REJ} limited, but not $Q_{REJ} \cdot L_{eff}$ limited. This could be considered evidence that the VCHP low heat transport problem was centered in the heat-exchanger-evaporator rather than in the VCHP condenser. Additional evidence was that at the design coolant flow rate the VCHP vapor temperature exceeded the coolant heat exchanger outlet temperature.

h. At this stage of its development the HPTRAN computer program has merit and is useful, but requires further validation. Some of this can be accomplished using the existing feasibility test data. For example, the $\Psi_{calc.}$ results for time period 193-07-03 to 193-08-36 are suspect. Final acceptance of the program awaits experimental data obtained on a VCHP with gas-vapor front locations that agreed much better with theoretical predictions.

i. The difference between the maximum and minimum panel temperatures between two active feeder heat pipes was consistently less in the feasibility tests than calculated. A detailed parametric study of the panel temperature distribution did not disclose any one reason for this test anomoly.

J. The computer models should be modified to consider the true feeder envelope and thereby a shorter panel fin length value than is currently used.

6.0 RECOMMENDATIONS FOR FUTURE STUDY

Based on the results of the studies described in this report, the following recommendations for future study can be made:

1. Determine why the feasibility VCHP was Q_{REJ} limited but not $Q_{REJ} \cdot L_{eff}$ limited.

2. The experimental transient behavior discussed in depth in Section 2.2 should be compared with the computer results from HPTRAN.

3. Continue with the validation of HPTRAN in the manner illustrated in Section 3.3. When the need for greater computer accuracy is justifiable, the number of VCHP nodal points should be increased.

4. Continue with the panel temperature distribution study to try to bring the analytical and experimental results into closer agreement.

7.0 REFERENCES

1. Sellers, J. P., Jr., "Steady State Operation of a Heat Pipe Radiator System: Analytical and Experimental", JSC-EC-R-74-1, L. B. Johnson Space Center, Dec. 1973.

2. Swerdling, B. and Alario, J., "Heat Pipe Radiator: Final Report", HPR-14, Grumman Aerospace Corporation, Oct. 1973.

3. Carroll, B. L., "User's Guide: Steady State Nodal Model of a Variable Conductance Heat Pipe Radiator System (PRFORM), "TM3045, Lockheed Electronic Company, Inc., Houston Aerospace Systems Division, July 1973.

4. Sadowski, B., "Data Memorandum: Heat Pipe Radiator", Environmental and Thermal Systems Engineering Branch, Crew Systems Division, L. B. Johnson Space Center, Feb. 1974.

5. Carroll, B. L., "User's Guide: Transient Variable Conductance Heat Pipe Radiator System (HPTRAN)", TM4016, Lockheed Electronic Company, Inc., Houston Aerospace Systems Division, Feb. 1974.

6. Carroll, B. L., "Correlation of Transient Heat Pipe Data with Computer Simulations from Program HPTRAN", TM4058, Lockheed Electronic Company, Inc., Houston Aerospace Systems Division, July 1974.

7. Adams, J. Alan, Rogers, David F., Computer Aided Heat Transfer Analysis, McGraw-Hill, 1973.

8.0 SYMBOLS

A	Area
C	Capacitance
C	T_i/T_E
C_p	Specific heat of the coolant
C1	Conductance
C2	Conductance
h_r	Radiation heat transfer coefficient
k	Thermal conductivity of panel
L_{eff}	$\frac{Lc}{2} + \frac{Lev}{2}$
L_{ca}	Length of the active portion of the VCHP condenser
L_{ev}	Length of the VCHP evaporator
$\dot{m}$	flow rate of the coolant
m_g	mass of the non-condensible gas
P_V	Pressure of the vapor in the VCHP
P_{VR}	Partial pressure of the vapor in the VCHP reservoir
P_{Vs}	Partial pressure of the vapor in the inactive portion of the VCHP
Q	Heat transport in a fully active feeder heat pipe
Q'_A	Absorbed heat flux
Q_{REJ}	Total heat removed from the coolant

Q_{rad}	Net heat radiated from panel
q	Heat transfer
R_g	Gas constant
t	Thickness of radiator panels
T_n	Temperature of the panel at a nodal point
T_{nR}	Temperature of the panel at a nodal point located on an active feeder heat pipe
T_i	Insulation temperature
T_{IN}	Temperature of the coolant as it enters the heat exchanger
T_{OUT}	Temperature of the coolant as it leaves the heat exchanger
T_{mean}	Logarithmic mean temperature between the coolant in the heat exchanger and T_V
T_V	Temperature of the vapor in the VCHP
T_E	Temperature of the environment
T_s	Temperature of the vapor and gas in the inactive portion of the VCHP condenser
T_R	Temperature of the reservoir
VCHP	Variable conductance heat pipe
V_R	Volume of the reservoir
V_c	Volume of the vapor in the VCHP condenser
x	Distance across the panel perpendicular to the feeder heat pipes
α	Absorptivity of the radiator panels

ΔT_p	$T_{n_R} - T_{n_{min}}$
ϵ, ϵ_1	Emissivity of the radiator panel
σ	Stefan-Boltzman constant
Ψ	Ratio of the active length to the total length of the VCHP condenser